



1           **Development of East Asia Regional**  
2           **Reanalysis based on advanced hybrid gain**  
3           **data assimilation method and evaluation**  
4           **with E3DVAR, ERA-5, and ERA-Interim**  
5           **reanalysis**

6  
7  
8  
9  
10  
11  
12  
13  
14  
15  
16

Eun-Gyeong Yang, Hyun Mee Kim\*, and Dae-Hui Kim

*Atmospheric Predictability and Data Assimilation Laboratory*

*Department of Atmospheric Science, Yonsei University, Seoul, Republic of Korea*

---

\* *Corresponding author address:* Hyun Mee Kim, Department of Atmospheric Sciences, Yonsei University, 50 Yonsei-ro, Seodaemun-gu, Seoul, 03722, Republic of Korea.

E-mail: [khm@yonsei.ac.kr](mailto:khm@yonsei.ac.kr)



17

## ABSTRACT

18           The East Asia Regional Reanalysis (EARR) system is developed based on the advanced  
19 hybrid gain data assimilation method (AdvHG) using Weather Research and Forecasting (WRF)  
20 model and conventional observations. Based on EARR, the high-resolution regional reanalysis  
21 and reforecast fields are produced with 12 km horizontal resolution over East Asia for 2010–  
22 2019. The newly proposed AdvHG is based on the hybrid gain approach, weighting two  
23 different analysis for an optimal analysis. The AdvHG is different from the hybrid gain in that  
24 1) E3DVAR is used instead of EnKF, 2) 6 h forecast of ERA5 is used to be more consistent  
25 with WRF, and 3) the pre-existing, state-of-the-art reanalysis is used. Thus, the AdvHG can be  
26 regarded as an efficient approach to generate regional reanalysis dataset due to cost savings as  
27 well as the use of the state-of-the-art reanalysis. The upper air variables of EARR are verified  
28 with those of ERA5 for January and July 2017 and the two-year period of 2017-2018. For upper  
29 air variables, ERA5 outperforms EARR over two years, whereas EARR outperforms (shows  
30 comparable performance to) ERA-I and E3DVAR for January in 2017 (July in 2017). EARR  
31 better represents precipitation than ERA5 for January and July in 2017. Therefore, though the  
32 uncertainties of upper air variables of EARR need to be considered when analyzing them, the  
33 precipitation of EARR is more accurate than that of ERA5 for both two seasons. The EARR  
34 data presented here can be downloaded from <https://doi.org/10.7910/DVN/7P8MZT> for data  
35 on pressure levels and <https://doi.org/10.7910/DVN/Q07VRC> for precipitation.

36



## 37 **1. Introduction**

38 Reanalysis datasets have been widely used in the socio-economical field as well as  
39 meteorological and climate research areas all over the world. Most of reanalysis datasets  
40 consist of global reanalysis whose spatial and temporal resolutions are relatively coarse (e.g.,  
41 Schubert et al. 1993; Kalnay et al. 1996; Gibson et al. 1997; Kistler et al. 2001; Kanamitsu et  
42 al. 2002; Uppala et al. 2005; Onogi et al. 2007; Bosilovich 2008; Saha et al. 2010; Dee et al.  
43 2011; Rienecker et al. 2011; Bosilovich 2015; Kobayashi et al. 2015; Hersbach et al. 2020). As  
44 the importance of regional reanalysis dataset emerged, many operational centers and research  
45 institutes around the world have been producing the dataset in their own areas (Mesinger et al.  
46 2006; Renshaw et al. 2013; Borsche et al. 2015; Bromwich et al. 2016; Jerney and Renshaw  
47 2016; Zhang et al. 2017; Bromwich et al. 2018; Fukui et al. 2018; Ashrit et al. 2020).

48 As part of this effort, regional reanalysis over East Asia were produced based on the  
49 Unified Model for the two-year period of 2013-14 and it was confirmed that regional reanalysis  
50 over East Asia is beneficial (Yang and Kim 2017; Yang and Kim 2019). However, because UM  
51 was no longer available for generating regional reanalysis over East Asia, another numerical  
52 weather prediction (NWP) model and its data assimilation (DA) method are required.

53 To find the most appropriate and cost-efficient DA method for a regional reanalysis over  
54 East Asia, several DA methods were compared. Yang and Kim (2021) demonstrated that the  
55 hybrid ensemble-variational data assimilation method (E3DVAR) shows the better  
56 performance compared to three-dimensional variational data assimilation (3DVAR) and  
57 ensemble Kalman filter (EnKF) over East Asia for January and July in 2016. However, it is  
58 essential to confirm if this hybrid method is accurate enough to be used for a regional reanalysis  
59 over East Asia. Thus, E3DVAR was compared with the latest and the previous reanalysis data  
60 from ECMWF (i.e., ECMWF's fifth-generation reanalysis (ERA5, Hersbach et al. 2020) and



61 ERA-Interim (ERA-I, Dee et al. 2011)) for (re)analysis and (re)forecast variables and it was  
62 found that a performance for a regional reanalysis needs to be further improved.

63 For this reason, a new advanced hybrid gain (AdvHG) data assimilation method, which  
64 combines E3DVAR and ERA5 based on WRF model, is newly proposed and investigated in  
65 this study. A hybrid gain data assimilation method has been developed as a new kind of hybrid  
66 methods (Penny 2014). Based on this method, an advanced data assimilation method is newly  
67 developed in this study. Finally, using this newly proposed DA method (AdvHG), East Asia  
68 regional reanalysis (EARR) system is developed based on WRF model. EARR datasets have  
69 been produced for ten-year period of 2010-2019 and are verified for two-year period of 2017–  
70 2018.

71 To investigate the accuracy and uncertainty of the state-of-the-art AdvHG DA algorithm  
72 developed in this study, analysis and forecast atmospheric variables of E3DVAR, AdvHG,  
73 WRF-based ERA-I, and WRF-based ERA5 are evaluated for January and July in 2017,  
74 respectively. In addition, reforecast precipitation fields of ERA-I and ERA5 from ECMWF are  
75 also verified and compared. In section 2, the EARR system including model, data assimilation  
76 method, and observations are explained. In section 3, the evaluation methods are presented.  
77 The verification results of (re)analysis and (re)forecast variables are presented in section 4.  
78 Section 4.1 presents evaluation results for wind, temperature, and humidity variables, and  
79 section 4.2 presents those for precipitation (re)forecast. Section 5 presents data availability.  
80 Lastly, summary and conclusions are presented in section 6.

## 81 **2. Reanalysis system**

### 82 *2.1. Model*

83 In this study, the Advanced Research Weather Research and Forecasting (WRF, v3.7.1)  
84 model is used with 12-km horizontal resolution (540 x 432 grid points) and 50 vertical levels



85 (up to 5 hPa) as shown in Fig. 1. The model settings and physics scheme are summarized in  
86 Table 1. Analysis fields are obtained every 6 h (00, 06, 12, and 18 UTC) via assimilation of  
87 conventional observations with a 6 h assimilation window, and forecast fields are integrated up  
88 to 36 h. The ERA5 reanalysis (Hersbach et al. 2020) is used as the first initial condition before  
89 the cycling, and as boundary conditions every 6 h.

## 90 2.2. Data assimilation methods

### 91 2.2.1. E3DVAR

92 The E3DVAR method is one of hybrid data assimilation methods, which use a static  
93 climatological background error covariance (BEC) and ensemble-based flow-dependent BEC,  
94 and couples the EnKF and 3DVAR (Zhang et al. 2013). E3DVAR is based on a cost function  
95 of 3DVAR. In E3DVAR, EnKF provides flow-dependent BEC as well as updates perturbations  
96 for ensemble members. Following Zhang et al. (2013),

$$J^b = J_s^b + J_e^b = \frac{1}{2} \delta \mathbf{x}^T \left[ (1 - \beta) \mathbf{B} + \beta \mathbf{P}^f \circ \mathbf{C} \right]^{-1} \delta \mathbf{x} , \quad (1)$$

97 where  $J_s^b$  is a traditional cost function based on a static climatological BEC  $\mathbf{B}$  and  $J_e^b$  is an  
98 additional cost function based on ensemble-based BEC  $\mathbf{P}^f$ .  $\mathbf{C}$  is a correlation matrix for  
99 localization of the ensemble covariance  $\mathbf{P}^f$ . The weighting coefficient  $\beta$  between static and  
100 ensemble-based BEC is set to 0.8 in this study. To account for model error for E3DVAR, multi-  
101 physics scheme is applied to 40-member ensembles. Yang and Kim (2021) found that E3DVAR  
102 is the most appropriate DA method among 3DVAR, EnKF, and E3DVAR methods over East  
103 Asia. More detailed information on E3DVAR implemented in this study can be found in Yang  
104 and Kim (2021).

### 105 2.2.2. Advanced hybrid gain data assimilation method

106 In the last decade, the traditional hybrid methods have been widely used for many  
107 operational centers and research institutes. Recently, Penny (2014) has proposed a new class



108 of hybrid gain methods combining desirable aspects of both variational and EnKF families of  
 109 algorithms by weighting analyses from 3DVAR and LETKF for an optimal analysis in the  
 110 Lorenz 40-component model. Since then, this algorithm has been implemented at ECMWF  
 111 (Bonavita et al. 2015) and at a hybrid global ocean DA system in National Centers for  
 112 Environmental Prediction (NCEP) (Penny et al. 2015).

113 The hybrid gain algorithm can be described with the following equations:

$$\mathbf{x}_{Hyb}^a = \alpha \mathbf{x}_{det}^a + (1 - \alpha) \overline{\mathbf{x}}^a, \quad (2)$$

114 where  $\mathbf{x}_{Hyb}^a$ ,  $\mathbf{x}_{det}^a$ , and  $\overline{\mathbf{x}}^a$  denote the hybrid analysis, deterministic analysis, and the ensemble  
 115 mean analysis from the ensemble-based assimilation method, and  $\alpha$  is a tunable parameter  
 116 (Penny 2014, Houtekamer and Zhang 2016).

117 The hybrid gain method is different from traditional hybrid methods, in that a hybrid gain  
 118 approach linearly combines analysis fields from EnKF and variational DA method to produce  
 119 a hybrid gain analysis rather than linearly combining respective BECs (Penny 2014). Basically,  
 120 the hybrid gain method is to hybridize two different Kalman gain matrices of ensemble-based  
 121 [Eq. (4)] and variational data assimilation system [Eq. (5)] as in Eq. (3).

$$\hat{\mathbf{K}} = \beta_1 \mathbf{K}^f + \beta_2 \mathbf{K}^B + \beta_3 \mathbf{K}^B \mathbf{H} \mathbf{K}^f, \quad (3)$$

122 where

$$\mathbf{K}^f = \mathbf{P}^f \mathbf{H}^T (\mathbf{H} \mathbf{P}^f \mathbf{H}^T + \mathbf{R})^{-1}, \quad (4)$$

$$\mathbf{K}^B = \mathbf{B} \mathbf{H}^T (\mathbf{H} \mathbf{B} \mathbf{H}^T + \mathbf{R})^{-1}. \quad (5)$$

123 By choosing the specific coefficients ( $\beta_1=1$ ,  $\beta_2 = \alpha$ ,  $\beta_3 = -\alpha$ ), it can be written as in Eq. (6)  
 124 and it can give an algebraically equivalent result with Eq. (2) (Penny 2014).

$$\hat{\mathbf{K}} = \mathbf{K}^f + \alpha \mathbf{K}^B (\mathbf{I} - \mathbf{H} \mathbf{K}^f). \quad (6)$$



125        One of advantages of the hybrid gain algorithm with respect to its development is that pre-  
126        existing operational systems can be used without significant modification for a hybrid analysis  
127        (Penny 2014) and independent parallel development of respective methods is allowed  
128        (Houtekamer and Zhang 2016). Furthermore, the hybrid gain approach can be considered as a  
129        practical and straightforward method in the foreseeable future to combine advantageous  
130        features of both ensemble- and variational-based DA algorithms (Houtekamer and Zhang 2016).  
131        More detailed information on this algorithm can be found in Penny (2014).

132        In this study, based on the hybrid gain approach, an advanced hybrid gain data assimilation  
133        method (AdvHG) is newly proposed as follows:

$$X_{\text{AdvHG}}^a = \alpha X_{\text{ERA5}}^{f(6h)} + (1 - \alpha) \bar{X}_{\text{E3DVAR}}^a, \quad (7)$$

134        where  $X_{\text{ERA5}}^{f(6h)}$  denotes the 6 h forecast of ERA5 reanalysis based on WRF model and  $\bar{X}_{\text{E3DVAR}}^a$   
135        denotes the analysis of E3DVAR. This advanced hybrid gain approach is different from the  
136        hybrid gain approach in that 1) E3DVAR analysis is used instead of EnKF, 2) 6 h forecast of  
137        ERA5 is used instead of deterministic analysis from variational DA method, and 3) the pre-  
138        existing and state-of-the-art reanalysis data (i.e., ERA5) is simply used instead of producing  
139        deterministic analysis by assimilation. The reasons for these different approaches proposed in  
140        this study are as follows:

141        1) E3DVAR is used instead of EnKF because Yang and Kim (2021) confirmed that  
142        E3DVAR outperforms EnKF for winter and summer seasons over East Asia.

143        2) Instead of deterministic analysis, the 6 h forecast of ERA5 based on WRF model is  
144        used to make the hybrid analysis more balanced and consistent with WRF model, because  
145        ERA5 reanalysis fields are based on its own modeling system with coarser resolution, which  
146        is different from that of this study.

147        3) European Centre for Medium-Range Weather Forecasts (ECMWF) reanalysis (ERA5)



148 is used instead of producing our own analysis fields from a variational DA method. This is a  
149 very efficient approach because of the cost savings as well as the use of the high-quality latest  
150 reanalysis from ECMWF assimilating all currently available observations with the state-of-the-  
151 art and advanced technology.

152 Therefore, the approach proposed in this study is called as “advanced hybrid gain method”  
153 (denoted as “AdvHG”).

### 154 *2.3. Observations*

155 The NCEP PrepBUFR conventional observations (global upper air and surface weather  
156 observations, NCEP/NWS/NOAA/U.S.DOC 2008) are used every 6 h (00, 06, 12, and 18 UTC)  
157 for an assimilation by E3DVAR and AdvHG methods. The assimilated observations are as  
158 follows: the surface observations (SYNOP, METAR, Ship, and Buoy), radiosonde observation  
159 (SOUND), upper-wind report (PILOT), wind profiler, aircraft, atmospheric motion vector  
160 (AMV) wind from a geostationary satellite (GEOAMV), and quick scatterometer (QuikSCAT).  
161 All observations are spatially thinned by 20 km except for AMV thinned by 200 km as done  
162 by Warrick (2015), Cotton et al. (2016), and Shin (2016).

163 To evaluate 6 h accumulated precipitation simulated by E3DVAR, AdvHG, ERA-I, and  
164 ERA5 over East Asia, global surface weather observations (NCEP PrepBUFR,  
165 NCEP/NWS/NOAA/U.S.DOC 2008) are used every 6 h (00, 06, 12, and 18 UTC). For an  
166 evaluation of the monthly precipitation fields, the world monthly surface station climatology  
167 (NCDC/NESDIS/NOAA/U.S.DOC et al. 1981) over 4700 different stations (2600 in more  
168 recent years) is used.

### 169 *2.4. Global reanalysis datasets*

170 To compare EARR generated with other reanalysis datasets, ERA5 (Hersbach et al. 2020)  
171 and ERA-I (Dee et al. 2011) reanalysis are chosen. The horizontal resolutions of ERA-I and  
172 ERA5 are approximately 79 km and 31 km, respectively. Because ERA5 is based on the



173 operational system in 2016, improvements in model physics, numerics, data assimilation, and  
174 additional observations over the last decade are the advantages of ERA5 (Hersbach et al. 2018).

175 Because reforecast as well as reanalysis fields are verified in this study, for forecast fields,  
176 two different forecast fields from ECMWF (i.e., forecast based on WRF model and reforecast  
177 based on ECMWF model) are used. The WRF forecast fields (i.e., WRF-based ERA5, WRF-  
178 based ERA-I) using ERA5 and ERA-I as initial conditions are integrated with 12 km resolution.  
179 Secondly, reforecast fields based on ECMWF model (i.e., ERA5\_fromECMWF, ERA-  
180 I\_fromECMWF), provided and downloaded from ECMWF, are used.

### 181 **3. Evaluation method**

#### 182 *3.1. Equitable threat score and Frequency bias index*

183 Based on the contingency table (Table 2), ETS is defined as

$$184 \text{ ETS} = \frac{A - A_r}{A + B + C - A_r}, \text{ where } A_r = \frac{(A + B)(A + C)}{A + B + C + D}. \quad (8)$$

184 The ETS range is from -1/3 to 1 and the value 1 for ETS is a perfect score.

185 FBI is defined as

$$186 \text{ FBI} = \text{Bias} = \frac{A + B}{A + C}. \quad (9)$$

186 The FBI indicates whether the model tends to over-forecast (too frequently, FBI>1) or under-  
187 forecast (not frequent enough, FBI<1) events with respect to frequency of occurrence.

#### 188 *3.2 Probability of detection and False alarm ratio*

189 Based on the contingency table (Table 2), POD is defined as

$$190 \text{ POD} = \frac{A}{A + C} = \frac{\text{Hits}}{\text{Hits} + \text{Misses}}. \quad (10)$$

190 The POD range is from 0 to 1. POD is required to be used with FAR, because POD can be  
191 artificially improved by systematically over-forecasting the events (Wilson 2010).



192 FAR is defined as

$$\text{FAR} = \frac{B}{A + B} = \frac{\text{False alarms}}{\text{Hits} + \text{False alarms}}. \quad (11)$$

193 The range of FAR is from 0 to 1 and its lower score implies a higher accuracy.

### 194 3.3 Brier skill score

195 Verification of the performance of high-resolution forecast with the traditional verification  
196 metrics (e.g., ETS, FBI) can be misleading due to double penalty, particularly for highly  
197 variable fields (e.g., precipitation). Therefore, as one of spatial verification approaches that do  
198 not require forecast to match point observation spatially, neighborhood (fuzzy) verification  
199 method, which assumes that slightly displaced forecast can be acceptable and a local  
200 neighborhood can define the degree of allowable displacement (Ebert 2008; Kim et al. 2015;  
201 On et al. 2018), is used in this section. According to Ebert (2008), depending on the matching  
202 strategy, neighborhood verifications can be categorized into two frameworks: ‘single  
203 observation-neighborhood forecast (SO-NF)’ where neighborhood forecasts surrounding  
204 observations are considered, and ‘neighborhood observation-neighborhood forecast (NO-NF)’  
205 strategies where not only neighborhood forecasts but also neighborhood observations  
206 surrounding observations are considered. Due to the absence of high-resolution gridded  
207 precipitation observation data in East Asia, various verification scores widely used as  
208 ‘neighborhood observation-neighborhood forecast (NO-NF)’ strategy are not available in this  
209 study. Thus, in this section, Brier skill score as one of ‘single observation-neighborhood  
210 forecast (SO-NF)’ strategy is introduced.

211 The Brier score (BS) is similar to the mean-squared error (MSE) and is defined as (Wilks  
212 2006):

$$\text{BS} = \frac{1}{N} \sum_{i=1}^N (p_i - o_i)^2. \quad (12)$$



213 where  $p_i$  denotes the probability forecast, and  $o_i$  denotes the binary observation which is either  
214 0 or 1, and  $N$  is the total number of observations during the given period. Generally, Brier skill  
215 score (or Brier score) is used to verify ensemble forecasts which are able to calculate  
216 probabilistic forecasts (Kay et al. 2013; Kim and Kim 2017). However, Brier skill score can  
217 also be used for deterministic forecasts using a pragmatic post-processing procedure (Theis et  
218 al., 2005; Mittermaier et al. 2014), which derives probabilistic forecasts from deterministic  
219 forecasts at every model grid point by considering neighborhood forecast as *pseudo ensemble*.

$$\text{BSS} = 1 - \frac{\text{BS}}{\text{BS}_{\text{ref}}}, \quad (13)$$

220 where  $\text{BS}_{\text{ref}}$  is Brier score of reference. Brier skill score is skill score with respect to Brier score  
221 as in Eq. (13). For reference, a climatology or other forecast can be used either. In this study,  
222 the WRF-based ERA-I is considered as a reference.

### 223 3.4 Pattern correlation coefficient

224 The pattern correlation coefficient (PCC) is defined as Eq. (14) (Shiferaw et al. 2018; Yoo  
225 and Cho 2018; Park and Kim 2020).

$$\text{PCC} = \frac{\sum_{i=1}^N (x_i - \bar{x})(o_i - \bar{o})}{\left[ \sum_{i=1}^N (x_i - \bar{x})^2 \sum_{i=1}^N (o_i - \bar{o})^2 \right]^{1/2}}, \quad (14)$$

226 where  $x_i$  and  $o_i$  are (re)forecast and observed precipitation at  $i$ th observation location and the  
227 over-bar indicates the averaged variables over  $N$  observed stations in the verification area.

## 228 4. Results

### 229 4.1 Evaluation of wind, temperature, and humidity variables

#### 230 4.1.1 RMSE for January and July 2017

231 The analysis and forecast RMSEs of E3DVAR, AdvHG, the WRF-based ERA-I, and



232 WRF-based ERA5 are calculated for zonal wind, meridional wind, temperature, and Qvapor  
233 (water vapor mixing ratio in WRF) variables against sonde observations at 00 and 12 UTC for  
234 January and July in 2017 and averaged over each month (Figs. 2, 3, and 4).

235 For analysis RMSE (Fig. 2), ERA5 is smaller than ERA-I for all levels and variables. In  
236 particular, the analysis RMSE difference between ERA5 and ERA-I is distinctive for wind. The  
237 vertically averaged wind RMSE of ERA5 for January ( $2.22 \text{ m s}^{-1}$ ) and July ( $1.98 \text{ m s}^{-1}$ ) in 2017  
238 is smaller by approximately  $0.23$  and  $0.3 \text{ m s}^{-1}$  than that of ERA-I for January ( $2.45 \text{ m s}^{-1}$ ) and  
239 July ( $2.28 \text{ m s}^{-1}$ ) in 2017. The analysis RMSE of E3DVAR is smaller than that of AdvHG for  
240 all pressure levels and variables, except for temperature in July at 1000 hPa and Qvapor in  
241 January and July at 1000 hPa. In general, the analysis RMSE of AdvHG for all variables is  
242 comparable to or greater than that of ERA5.

243 Regarding wind variables of analysis (Figs. 2a, b, c, and d), E3DVAR is the most closely  
244 fitted to observations except for the wind in upper troposphere in January, followed by ERA5,  
245 AdvHG, and ERA-I. For temperature RMSE (Figs. 2e and f), E3DVAR is smaller than AdvHG  
246 and ERA5 is smaller than ERA-I. However, in January (Fig. 2e), ERA5 RMSE is the smallest  
247 for upper troposphere and RMSEs of ERA5 and E3DVAR are similar to each other for lower  
248 troposphere. In July (Fig. 2f), overall E3DVAR RMSE is the smallest except for 1000 hPa. For  
249 Qvapor, RMSE in July is much larger than that in January due to a monsoonal flow carrying  
250 moist air to East Asia. In general, Qvapor RMSE of E3DVAR is the smallest, followed by  
251 ERA5, AdvHG, and ERA-I. Therefore, for all variables, generally E3DVAR analysis fields are  
252 the most closely fitted to observations. Since the analysis RMSE implies how much analysis  
253 fields are fitted to observations rather than the accuracy of analysis itself, not only analysis  
254 RMSE but also forecast RMSE should be considered.

255 For 24 h forecast RMSEs (Fig. 3), ERA5 RMSE is the smallest for all levels and variables  
256 for January and July in 2017. In January (Figs. 3a, c, e, and g), overall, the 24 h forecast RMSE



257 of ERA5 is the smallest and that of ERA-I is the largest for all variables, and RMSEs of AdvHG  
258 and E3DVAR are greater than those of ERA5 and smaller than those of ERA-I. Regarding  
259 AdvHG and E3DVAR, in general, AdvHG is smaller than E3DVAR for all levels and variables.  
260 Thus, in January, ERA5 is the most accurate, followed by AdvHG, E3DVAR, and ERA-I.  
261 Meanwhile, for July (Figs. 3b, d, f, and h), ERA5 shows the smallest RMSE, and AdvHG and  
262 E3DVAR show comparable RMSE to ERA-I.

263 Furthermore, general features of 36 h forecast RMSE (Fig. 4) are similar to the 24 h  
264 forecast RMSE (Fig. 3). However, particularly in January, the 36 h forecast RMSE differences  
265 between ERA5 and ERA-I are more distinctive compared to those of 24 h forecast. In January,  
266 the vertically averaged 36 h forecast RMSE differences of ERA5 and ERA-I are  $0.52 \text{ m s}^{-1}$  for  
267 wind,  $0.16 \text{ K}$  for temperature, and  $0.08 \text{ g kg}^{-1}$  for Qvapor, whereas those of 24 h forecast are  
268  $0.4 \text{ m s}^{-1}$  for wind,  $0.11 \text{ K}$  for temperature, and  $0.06 \text{ g kg}^{-1}$  for Qvapor. In addition, the 36 h  
269 forecast RMSE differences between ERA5 and AdvHG for January are on average  $0.1 \text{ m s}^{-1}$   
270 for wind,  $0.05 \text{ K}$  for temperature, and  $0.02 \text{ g kg}^{-1}$  for Qvapor, which are even smaller compared  
271 to those of 24 h forecast, implying that AdvHG is a lot more accurate than ERA-I for January  
272 in 2017. For July, 36 h forecast RMSE of ERA5 is the smallest and RMSEs of AdvHG and  
273 E3DVAR are similar to those of ERA-I.

#### 274 4.1.2 RMSE and spread for the period of 2017-18

275 In this section, EARR produced in this study is verified for a longer period with WRF-  
276 based ERA5. RMSE and spread of reanalyses and reforecasts based on AdvHG method are  
277 calculated and averaged over the period of 2017–2018. The reanalyses and (re)forecast fields  
278 are evaluated by calculating RMSE valid at 00 and 12 UTC and spread at 00, 06, 12, and 18  
279 UTC.

280 The averaged RMSEs of reanalysis for ERA5 and EARR (denoted as AdvHG in Fig. 5)  
281 and spread of analysis and 6 h forecast fields of EARR (AdvHG) are shown in Fig. 5. With



282 respect to spread, the ensemble spreads of analysis fields are smaller than those of 6 h forecast  
283 fields, on average, by  $0.16 \text{ m s}^{-1}$  for wind,  $0.04 \text{ K}$  for temperature, and  $0.02 \text{ g kg}^{-1}$  for Qvapor,  
284 which is the well-known characteristics of ensemble-based data assimilation methods. To be  
285 specific, the wind spread (Figs. 5a and b) is similar to or greater than the wind RMSE except  
286 for the upper troposphere above 200 hPa, implying ensemble spread for wind is well  
287 represented below 200 hPa. Even if the ensembles for temperature (Fig. 5c) are underdispersive  
288 compared to RMSE of temperature, overall Qvapor spread (Fig. 5d) is well represented except  
289 for 1000 hPa and above 200 hPa.

290 Regarding reanalysis RMSE, overall ERA5 RMSE is smaller than AdvHG RMSE for all  
291 variables (Fig. 5). The vertically averaged RMSEs of ERA5 are smaller by  $0.15 \text{ m s}^{-1}$  for wind,  
292  $0.08 \text{ K}$  for temperature, and  $0.01 \text{ g kg}^{-1}$  for Qvapor than those of AdvHG. Nonetheless, the  
293 wind RMSEs of AdvHG are similar to those of ERA5 for the middle of troposphere (400–850  
294 hPa), and the Qvapor RMSEs of AdvHG are similar to those of ERA5 except for 1000 hPa.

295 In addition, regarding 24 h forecast RMSE, ERA5 shows smaller RMSE than AdvHG for  
296 all variables (Fig. 6). The vertically-averaged RMSE differences of wind, temperature, and  
297 Qvapor variables between AdvHG and ERA5 are approximately  $0.2 \text{ m s}^{-1}$ ,  $0.07 \text{ K}$ , and  $0.03 \text{ g}$   
298  $\text{kg}^{-1}$ , respectively. These differences are smaller, compared to the 24 h forecast RMSE  
299 difference between ERA-I and ERA5 shown in Fig. 3 (i.e., wind, Temp, and Qvapor RMSE  
300 difference:  $0.4 \text{ m s}^{-1}$ ,  $0.11 \text{ K}$ , and  $0.06 \text{ g kg}^{-1}$  for January 2017,  $0.25 \text{ m s}^{-1}$ ,  $0.05 \text{ K}$ , and  $0.04 \text{ g}$   
301  $\text{kg}^{-1}$  for July 2017).

## 302 4.2 Evaluation of precipitation for January and July in 2017.

### 303 4.2.1 Evaluation metrics

#### 304 4.2.1.1 Equitable threat score and Frequency bias index

305 In this section, for the point-based Equitable threat score (ETS) and Frequency bias index  
306 (FBI) based on Table 2, the 6 h accumulated precipitation fields based on the 6 h forecast of



307 E3DVAR, AdvHG, WRF-based ERA-I, WRF-based ERA5, ERA-I\_fromECMWF, and  
308 ERA5\_fromECMWF are evaluated every 6 h (00, 06, 12, and 18 UTC) for January and July in  
309 2017 (Fig. 7). Here, all the WRF-based precipitation fields are based on 12-km horizontal  
310 resolution, and ERA-I\_fromECMWF and ERA5\_fromECMWF have 79- and 31-km horizontal  
311 resolutions, respectively. Generally, ETS decreases as a threshold increases for both two  
312 months (Figs. 7a and c). For January in 2017 (Fig. 7a), AdvHG ETS is the greatest among  
313 others. Compared to precipitation reforecasts from ECMWF (i.e., ERA-I\_fromECMWF,  
314 ERA5\_fromECMWF), AdvHG shows the higher ETS, indicating that AdvHG is able to  
315 simulate more accurate precipitation fields than ERA-I and ERA5 from ECMWF in January  
316 2017. Surprisingly, ETS of ERA5\_fromECMWF for January in 2017 is the lowest among all  
317 the results compared and is even lower than that of ERA-I\_fromECMWF.

318       Since the precipitation reforecasts from ECMWF have not only coarser resolutions but  
319 also different forecast model (i.e., the forecasting system of ECMWF), the precipitation  
320 forecasts of ERA5 and ERA-I are additionally produced by using the same forecast model with  
321 the same resolution as AdvHG and E3DVAR in this study, as explained in section 2.4. For  
322 January 2017 (Fig. 7a), ETS of ERA5 (i.e., WRF-based ERA5) is higher than that of  
323 ERA5\_fromECMWF for all thresholds, whereas ETS of ERA-I (i.e., WRF-based ERA-I) is  
324 lower than that of ERA-I\_fromECMWF except for strong thresholds. The ERA5 ETS is greater  
325 than the ERA-I ETS, but is smaller than the AdvHG ETS. The AdvHG shows the greatest ETS  
326 among others with the same resolution and forecast model, and E3DVAR, ERA5, and ERA-I  
327 follow.

328       Regarding FBI in winter (Fig. 7b), for strong thresholds, all the results show the FBI  
329 smaller than 1, implying the underestimation of frequency of precipitation for strong thresholds.  
330 While FBIs of ERA5\_fromECMWF and ERA-I\_fromECMWF are greater than 1 for weak  
331 thresholds, those WRF-based results are similar to 1 or smaller than 1. In general, AdvHG



332 shows the FBI closest to 1 among all the results, which is consistent with the greatest ETS of  
333 AdvHG. The E3DVAR FBI is similar to the AdvHG FBI, and ERA5 and ERA-I FBIs are  
334 similar to each other. FBIs of ERA5 and ERA-I are smaller than those of AdvHG and E3DVAR.

335 Meanwhile, overall, the ETS values for January whose maximum is around 0.4 (Fig. 7a)  
336 are much greater than those for July in 2017 whose maximum is around 0.2 (Fig. 7c), implying  
337 that the precipitation forecast in summer is more difficult than that in winter. The ETS  
338 difference between the results in July is smaller than those in January. Particularly, for the  
339 thresholds 4 and 8 mm (6 h)<sup>-1</sup>, ETSs in July are similar to each other (Fig. 7c). Except for those  
340 two thresholds, the ETS of ERA-I\_fromECMWF is the smallest. At the threshold 16 mm (6 h)<sup>-1</sup>,  
341 ERA5 ETS is the highest, followed by AdvHG, E3DVAR, ERA-I, ERA5\_fromECMWF, and  
342 ERA-I\_fromECMWF. At the threshold 0.5 and 1 mm (6 h)<sup>-1</sup>, the E3DVAR ETS is the greatest,  
343 followed by ERA5, AdvHG, ERA5\_fromECMWF, ERA-I, and ERA-I\_fromECMWF.

344 With respect to FBI in July 2017, the WRF-based results show the FBIs greater than 1,  
345 whereas reforecast from ECMWF show the FBIs greater than 1 for weak thresholds and smaller  
346 than 1 for strong thresholds (Fig. 7d). For July in 2017, in general, ERA5\_fromECMWF FBI  
347 is the closest to 1, followed by E3DVAR, AdvHG, ERA5, ERA-I, and ERA-I\_fromECMWF  
348 FBI.

#### 349 *4.2.1.2 Probability of detection and False alarm ratio*

350 The Probability of Detection (POD or Hit Rate) and False Alarm Ratio (FAR) are  
351 calculated for precipitation simulated from E3DVAR, AdvHG, WRF-based ERA-I, WRF-  
352 based ERA5, ERA-I\_fromECMWF, and ERA5\_fromECMWF for January and July in 2017  
353 (Fig. 8). For January in 2017, AdvHG POD is the greatest among the WRF-based results,  
354 followed by E3DVAR, ERA5, and ERA-I (Figs. 8a and b). Overall, the results of reforecast  
355 from ECMWF (i.e., ERA-I\_fromECMWF and ERA5\_fromECMWF) have greater POD than  
356 the WRF-based POD for weak thresholds, whereas those have smaller POD than the WRF-



357 based POD for strong thresholds. Regarding FAR, notably, ERA5\_fromECMWF shows  
358 extremely great FAR and ERA5 shows the smallest FAR among all the results, which is a  
359 consistent result with the smallest ETS of ERA5\_fromECMWF. In addition to the lowest ETS  
360 of ERA5\_fromECMWF for January in 2017 as discussed in the section 4.2.1.1, FAR of  
361 ERA5\_fromECMWF is extremely high with low POD in winter. Therefore, especially for  
362 January in 2017, the precipitation fields simulated from ERA5\_fromECMWF over East Asia  
363 are much less accurate than any other results from this study.

364 For July in 2017, generally, ERA5 shows the largest POD, followed by AdvHG, ERA-I,  
365 E3DVAR, ERA5\_fromECMWF (Figs. 8c and d). The ERA-I POD shows the largest POD for  
366 weak thresholds and the smallest POD for strong thresholds, compared to other results. With  
367 respect to FAR, FAR values in July is much greater than those in January, which is consistent  
368 with the ETS difference between these two seasons. Overall, for strong thresholds, ERA-I  
369 shows the highest FAR and ERA-I\_fromECMWF shows the smallest FAR. For weak  
370 thresholds, the ERA-I\_fromECMWF shows the highest FAR and E3DVAR shows the smallest  
371 FAR among all the results.

#### 372 *4.2.1.3 Brier skill score*

373 The neighborhood sizes are chosen to be  $3\Delta x$ ,  $5\Delta x$ ,  $9\Delta x$ , and  $11\Delta x$ , which are 36, 60,  
374 108, and 132 km, respectively, and the thresholds  $0.5$ ,  $1$ ,  $4$ ,  $8$ , and  $16 \text{ mm (6 h)}^{-1}$  are considered.  
375 The probabilistic precipitation forecasts are calculated at every model grid point depending on  
376 neighborhood sizes and thresholds. Regarding each observation, the nearest model grid point  
377 to observations is considered as the center of neighborhood. For verification, 6 h accumulated  
378 precipitation fields are extracted from the first 0–6 h forecast fields of WRF-based ERA-I,  
379 WRF-based ERA5, E3DVAR, and AdvHG every 6 h (00, 06, 12, and 18 UTC). BSSs of  
380 ERA5\_fromECMWF and ERA-I\_fromECMWF are not calculated, because they have different  
381 resolution from WRF-based results.



382       Based on the neighborhood approach, Brier skill score (BSS) is calculated depending on  
383 different neighborhood sizes for January and July in 2017, respectively (Fig. 9). Because the  
384 reference of Brier score is chosen as the ERA-I, the positive BSS implies better accuracy than  
385 ERA-I. In general, for both two months, AdvHG BSS is greater than ERA5 BSS. Although the  
386 E3DVAR BSS is the greatest in July 2017, the AdvHG BSS is the greatest in January 2017.

387       For January in 2017, as a neighborhood size increases, AdvHG and E3DVAR BSSs tend  
388 to increase except for ERA5. Overall, AdvHG BSS is the greatest among other BSSs for all  
389 thresholds for all neighborhood sizes. The ERA5 BSS is greater than E3DVAR BSS except for  
390  $16 \text{ mm } (6 \text{ h})^{-1}$ . The highest BSS of AdvHG and the lowest BSS of ERA-I are consistent with  
391 ETS result. Unlike greater E3DVAR ETS than ERA5 ETS, ERA5 BSS is greater than E3DVAR  
392 BSS in January 2017.

393       For July 2017, while the ETS difference between the WRF-based results is not distinct  
394 (Fig. 7c), the BSS difference is rather noticeable. Generally, E3DVAR BSS is the greatest  
395 among other BSSs for all thresholds except for  $16 \text{ mm } (6 \text{ h})^{-1}$  for neighborhood sizes 9 and 11.  
396 Although E3DVAR BSS is the largest, AdvHG outperforms ERA5 and ERA-I. The worst  
397 performance of ERA-I precipitation is consistent with ETS result. At weak thresholds,  
398 E3DVAR BSS is the greatest, which is similar to ETS. For strong thresholds, ERA5 ETS is the  
399 highest, followed by AdvHG and E3DVAR, whereas overall E3DVAR BSS is the highest,  
400 followed by AdvHG and ERA5.

#### 401 *4.2.2 Spatial distribution*

##### 402 *4.2.2.1 6 h accumulated precipitation with the pattern correlation coefficient*

403       In this section, the spatial distributions of 6 h accumulated precipitation from the WRF-  
404 based forecast and reforecast from ECMWF are compared. In addition, pattern correlation  
405 coefficients (PCC) are calculated and shown at the bottom right of Figs. 10 and 11.

406       The PCC is computed according to the usual Pearson correlation operating on the N



407 observed point pairs of 6 h accumulated precipitation fields simulated from (re)forecast and  
408 observations at the specific time. For the calculation of PCC, 6 h accumulated precipitation  
409 fields from (re)forecast fields are interpolated bilinearly to the N observed points.

410 Firstly, on 29<sup>th</sup> and 30<sup>th</sup> of January in 2017 (Fig. 10), it is noticeable that the precipitation  
411 of ERA5\_fromECMWF does not match observations well over East Asia compared to other  
412 simulated precipitation fields. As shown in Fig. 10g, ERA5\_fromECMWF incorrectly  
413 simulates precipitation over South East China, whereas other results do not forecast  
414 precipitation over this area. In addition, ERA5\_fromECMWF overestimates precipitation over  
415 inland area of China (Fig. 10zz), whereas other results simulate precipitation similar to  
416 observations regarding its position and intensity. ERA5\_fromECMWF also shows noticeably  
417 smaller PCC (Figs. 10g, n, and zz). Although PCC does not represent the exact accuracy or  
418 predictability of precipitation, the overall feature of PCC is consistent with the results found so  
419 far. In particular, PCCs of ERA5\_fromECMWF are much smaller than those of other  
420 precipitation fields. For January in 2017, the averaged PCC of AdvHG is the greatest (i.e., 0.61)  
421 and that of ERA5\_fromECMWF is the smallest (i.e., 0.46) (not shown).

422 Secondly, for 1<sup>st</sup> and 2<sup>nd</sup> of July in 2017 (Fig. 11), overall, the precipitation simulated from  
423 ERA5\_fromECMWF is well represented, compared to January in 2017 shown in Fig. 10. The  
424 ERA-I\_fromECMWF fails to simulate heavy rain for summer season due to its coarse  
425 resolution. Furthermore, during July in 2017, ERA5 and ERA-I simulate heavier precipitation  
426 than AdvHG (not shown), which is consistent with larger FBI of ERA5 and ERA-I at strong  
427 thresholds. For one-month period of July in 2017, the averaged PCC of ERA5 is the greatest  
428 (i.e., 0.37) and that of AdvHG is 0.34, but the PCC difference between ERA5 and AdvHG is  
429 not distinctive. Moreover, the overall range of averaged PCC of different datasets in summer  
430 (i.e., 0.29-0.35) is smaller than that in winter (i.e., 0.46-0.61), which is consistent with the  
431 seasonal difference of ETS in this study.



432 *4.2.2.2 Monthly accumulated precipitation*

433 In this section, the monthly accumulated precipitation fields of rain gauge based  
434 observations, E3DVAR, AdvHG, ERA-I, ERA5, ERA-I\_fromECMWF, and  
435 ERA5\_fromECMWF are compared to each other for two one-month periods in January and  
436 July in 2017, respectively.

437 Although all the results similarly represent overall features of precipitation in January (Fig.  
438 12), ERA5\_fromECMWF (Fig. 12g) simulates the overestimated precipitation over South  
439 China, compared to other results and observations, which is consistent with the results in the  
440 previous section as well as its larger FBI at weak thresholds shown in Fig. 7b. It is noticeable  
441 that all results fail to represent the observed precipitation area over Tibetan Plateau (25°–40°N,  
442 95°–105°E). The monthly accumulated precipitation fields simulated by E3DVAR and AdvHG  
443 (Figs. 12 b and c) are similar to each other, and E3DVAR and AdvHG produce the best fit to  
444 observed fields. Especially, for the north-western part of Japan (e.g., Chugoku and Kinki),  
445 E3DVAR and AdvHG are able to represent precipitation correctly, whereas ERA-  
446 I\_fromECMWF and ERA5\_fromECMWF fail to do so (Fig. 12).

447 For the monthly accumulated precipitation in July 2017, overall, the ERA5\_fromECMWF  
448 (Fig. 13g) and the WRF-based results (Fig. 13b, c, and e) except for ERA-I (Fig. 13d) well  
449 simulate precipitation similar to observations. ERA-I\_fromECMWF is not able to simulate  
450 heavy precipitation over Korea. For western and southern part of Japan, while ERA-  
451 I\_fromECMWF and ERA5\_fromECMWF simulate similar precipitation fields to observed  
452 fields, WRF-based results overestimate precipitation over these regions. Compared to ERA-  
453 I\_fromECMWF and ERA5\_fromECMWF, the WRF-based results tend to overestimate  
454 precipitation in South China, Korea, and Japan. This is consistent with the result in Fig. 7d, in  
455 which FBIs from WRF-based results are generally greater than 1 for strong thresholds, whereas  
456 those from ECMWF are smaller than 1.



457 Even though detailed precipitation features of WRF-based results are different, overall  
458 features of precipitation from WRF-based results are similar to each other, which implies that  
459 predictability of precipitation strongly depend on the physics schemes as well as NWP model,  
460 especially for summer season. According to Que et al. (2016), depending on the combinations  
461 of physics options in WRF model, the spatial distribution of precipitation can be significantly  
462 different over Asian summer monsoon area and YSU PBL scheme which is used in this study  
463 tends to overestimate precipitation over the same area. Thus, different physics options could  
464 simulate the different spatial distribution of precipitation.

465 In addition, compared to ERA5 based on WRF model (Fig. 13e), ECMWF model for  
466 ERA5\_fromECMWF (Fig. 13g) seems to suppress precipitation. Thus, WRF model with the  
467 physics schemes used in this study might simulate more precipitation than ECMWF model,  
468 although the initial condition is the same. Therefore, it is important to consider the consistency  
469 of the systems for data assimilation and forecast model for a good performance of precipitation.

## 470 **5. Data Availability**

471 The EARR data presented in this study are available every 6 h (i.e., 00, 06, 12, and 18  
472 UTC) for the period of 2010-2019 from Harvard Dataverse Repository  
473 (<https://dataverse.harvard.edu/dataverse/EARR>). The EARR 6 hourly data on pressure levels  
474 (<https://doi.org/10.7910/DVN/7P8MZT>, Yang and Kim 2021b) and 6 hourly precipitation data  
475 (<https://doi.org/10.7910/DVN/Q07VRC>, Yang and Kim 2021c) are provided in NetCDF file  
476 format.

477 The EARR 6 hourly data on pressure levels (Yang and Kim 2021b) include u-component  
478 of wind, v-component of wind, temperature, geopotential height, and specific humidity  
479 variables of reanalysis on pressure levels (i.e., 925, 850, 700, 500, 300, 200, 100, and 50 hPa).  
480 The EARR 6 hourly precipitation data (Yang and Kim 2021c) contain 6 h accumulated total



481 precipitation variable of 6 h reforecast on single level. The 6 h accumulated total precipitation  
482 is obtained from 6 h reforecast field which is integrated for 6 h from reanalysis field every 6 h  
483 (i.e., 00, 06, 12 and 18 UTC).

## 484 **6. Summary and conclusions**

485 In this study, to develop the regional reanalysis system over East Asia, the advanced  
486 hybrid gain algorithm (AdvHG) is newly proposed and evaluated with traditional hybrid DA  
487 method (E3DVAR) as well as existing reanalyses from ECMWF (ERA5 and ERA-I) for  
488 January and July in 2017. The East Asia Regional Reanalysis (EARR) system is developed  
489 based on the AdvHG as the data assimilation method using WRF model and conventional  
490 observations, and the high-resolution regional reanalysis and reforecast fields with 12 km  
491 horizontal resolution are produced over East Asia for the ten-year period of 2010–2019.

492 The AdvHG newly proposed in this study is based on the hybrid gain approach, weighting  
493 analysis from variational-based and ensemble-based DA algorithms to generate optimal hybrid  
494 analysis, which can play an important role as a simple and practical method in the foreseeable  
495 future to take advantage of each strength of two different methods. The advanced hybrid gain  
496 method is different from the hybrid gain approach in that 1) E3DVAR is used instead of EnKF,  
497 2) 6 h forecast of ERA5 is used instead of deterministic analysis for a more balanced and  
498 consistent analysis with WRF model, and 3) the pre-existing and state-of-the-art reanalysis data  
499 (i.e. ERA5) is simply used instead of producing our own analysis fields from a variational DA  
500 method. Thus, it can be regarded as an efficient approach to generate regional reanalysis dataset  
501 because of cost savings as well as the use of the state-of-the-art reanalysis from ECMWF that  
502 assimilates all available observations.

503 For a verification, the latest ECMWF reanalysis and reforecast datasets (i.e., ERA5 and  
504 ERA-I) are used. With respect to forecast variables, two different forecast fields of ECWMF



505 are used: 1) reforecast fields from ECMWF (i.e., ERA5\_fromECMWF and ERA-  
506 I\_fromECMWF) and 2) forecast fields (i.e., WRF-based ERA5 and WRF-based ERA-I)  
507 integrated in WRF model with 12 km resolution using ERA5 and ERA-I as initial conditions.

508 To evaluate this newly proposed algorithm, analysis and forecast wind, temperature, and  
509 humidity variables are evaluated with respect to RMSE and spread for January and July in 2017.  
510 Overall, the analysis RMSE of E3DVAR is the smallest among others but comparable to that  
511 of ERA5, especially for January. Regarding forecast variables, AdvHG outperforms E3DVAR  
512 and ERA5 outperforms ERA-I for January and July in 2017. Although ERA5 outperforms  
513 AdvHG for upper air variables for two seasons, AdvHG outperforms ERA-I in January and  
514 shows comparable performance to ERA-I in July. Additionally the verification results of  
515 AdvHG and ERA5 for the period of 2017-18 are consistent with those for two one-month  
516 period in 2017.

517 The precipitation forecast variables are also verified regarding a neighborhood-based  
518 verification score (i.e., Brier skill score) as well as the point-based verification scores (i.e., ETS,  
519 FBI, POD, and FAR). According to the point-based verification scores, the precipitation  
520 forecast of AdvHG in January is the most accurate, followed by E3DVAR, ERA5, ERA-I. The  
521 precipitation reforecast of ERA5\_fromECMWF shows the worst performance with the lowest  
522 ETS and the highest FAR among other results in January. For July, overall ETS values of all  
523 results are relatively lower compared to those in January, implying the lower predictability in  
524 summer season. For July, ERA5 shows the greatest ETS for strong thresholds followed by  
525 AdvHG and E3DVAR, and E3DVAR ETS is the greatest followed by ERA5 and AdvHG for  
526 weak thresholds. However, the ETS differences between the results are not distinctive.

527 To prevent from double penalty when verifying a highly variable data with high resolution  
528 (e.g., precipitation), Brier skill score (BSS) based on neighborhood approach is calculated for  
529 6 h accumulated precipitation forecasts depending on different neighborhood sizes for January



530 and July in 2017. In general, BSS of AdvHG is greater than that of ERA5 and ERA-I for both  
531 two months. Although the E3DVAR BSS is the greatest in July 2017, the AdvHG BSS is the  
532 greatest in January 2017.

533 Lastly, the spatial distributions of 6 h and monthly accumulated precipitation forecast for  
534 AdvHG, E3DVAR, ERA-I, ERA5, ERA-I\_fromECMWF, and ERA5\_fromECMWF are  
535 compared with rain-gauge based observations. For January 2017, it is noticeable that AdvHG  
536 precipitation is the closest to observations with highest PCC (i.e., 0.61) and  
537 ERA5\_fromECMWF overestimates precipitation over South China with the lowest PCC (i.e.,  
538 0.46). For July in 2017, due to a coarse resolution of ERA-I\_fromECMWF, it fails to represent  
539 heavy rain over East Asia. Meanwhile, the WRF-based results tend to overestimate  
540 precipitation compared to ERA-I\_fromECMWF and ERA5\_fromECMWF. In addition, even  
541 though the averaged PCC of ERA5 (i.e., 0.37) is slightly greater than that of AdvHG (i.e., 0.34),  
542 the PCC difference between ERA5 and AdvHG is not distinctive and overall range of averaged  
543 PCC of all datasets in summer (i.e., 0.29-0.35) is smaller than that in winter (i.e., 0.46-0.6).

544 In conclusion, for upper air variables, overall, ERA5 outperforms EARR based on AdvHG,  
545 but the RMSE difference between ERA5 and EARR (AdvHG) is smaller than that between  
546 ERA5 and ERA-I. In addition, EARR outperforms ERA-I for January 2017 and shows  
547 comparable performance to ERA-I for July 2017. On the contrary, according to the evaluation  
548 results of precipitation, in general, EARR better represents precipitation than ERA5 as well as  
549 ERA5\_fromECMWF for January and July in 2017. Even if E3DVAR precipitation is better  
550 represented than EARR precipitation for July, the difference is not considerable for July and  
551 EARR better simulates precipitation for January than E3DVAR. Therefore, although the  
552 uncertainties of upper air variables of EARR should be considered when analyzing them, the  
553 precipitation reforecast of EARR is more accurate than that of ERA5 for both two seasons.

554



555 **Author contribution**

556 Hyun Mee Kim proposed the main scientific ideas and Eun-Gyeong Yang contributed the  
557 supplementary ideas during the process. Eun-Gyeong Yang developed the reanalysis system  
558 and produced the 10-year regional reanalysis data. Eun-Gyeong Yang and Hyun Mee Kim  
559 analyzed the simulation results and completed the manuscript. Dae-Hui Kim contributed to  
560 analyzing the reanalysis data and to the preparation of software and computing resources for  
561 the reanalysis system.

562

563 **Competing interests**

564 The authors declare that they have no competing interests.

565

566 **Acknowledgments**

567 This study was supported by a National Research Foundation of Korea (NRF) grant funded by  
568 the South Korean government (Ministry of Science and ICT) (Grant 2017R1E1A1A03070968  
569 and Grant 2021R1A2C1012572) and the Yonsei Signature Research Cluster Program of 2021  
570 (2021-22-0003). This study was carried out by utilizing the supercomputer system supported  
571 by the National Center for Meteorological Supercomputer of Korea Meteorological  
572 Administration and Korea Research Environment Open NETWORK (KREONET) provided by  
573 the Korea Institute of Science and Technology Information. The authors gratefully  
574 acknowledge the late Dr. Fuqing Zhang for collaborations at the earlier stages of this study.

575

576



577 **References**

- 578 Ashrit, R., S. Indira Rani, S. Kumar, S. Karunasagar, T. Arulalan, T. Francis, A. Routray, S. I. Laskar,  
579 S. Mahmood, P. Jerney, A. Maycock, R. Renshaw, J. P. George, and E. N. Rajagopal, 2020:  
580 IMDAA Regional Reanalysis: Performance Evaluation During Indian Summer Monsoon  
581 Season. *Journal of Geophysical Research: Atmospheres*, **125**(2), e2019JD030973.
- 582 Bonavita, M., M. Hamrud, and L. Isaksen, 2015: EnKF and hybrid gain ensemble data assimilation.  
583 Part II: EnKF and hybrid gain results. *Monthly Weather Review*, **143**(12), 4865-4882.
- 584 Borsche, M, A. K. Kaiser-Weiss, P. Undén, and F. Kaspar, 2015: Methodologies to characterize  
585 uncertainties in regional reanalyses. *Adv. Sci. Res.*, **12**, 207-218.
- 586 Bosilovich, M., 2008: NASA's modern era retrospective-analysis for research and applications:  
587 Integrating Earth observations. Earthzine, 26 September 2008. [Available online at  
588 [www.earthzine.org/2008/09/26/nasas-modern-era-retrospective-analysis/](http://www.earthzine.org/2008/09/26/nasas-modern-era-retrospective-analysis/).]
- 589 Bosilovich, M., R. Lucchesi, and M. Suarez, 2015: MERRA-2: File specification. NASA GMAO Office  
590 Note 9, 73 pp., <http://gmao.gsfc.nasa.gov/pubs/docs/Bosilovich785.pdf>.
- 591 Bromwich, D. H., A. B. Wilson, L. Bai, Z. Liu, M. Barlage, C. F. Shih, S. Maldonado, K. M. Hines, S.-  
592 H. Wang, J. Woollen, B. Kuo, H.-C. Lin, T.-K. Wee, M. C. Serreze, and J. E. Walsh, 2018: The  
593 Arctic system reanalysis, version 2. *Bulletin of the American Meteorological Society*, **99**(4),  
594 805-828.
- 595 Bromwich, D. H., A. B. Wilson, L. S. Bai, G. W. Moore, and P. Bauer, 2016: A comparison of the  
596 regional Arctic System Reanalysis and the global ERA-Interim Reanalysis for the Arctic.  
597 *Quarterly Journal of the Royal Meteorological Society*, **142**(695), 644-658.
- 598 Cotton, J., M. Forsythe, F. Warrick, K. Salonen, N. Bormann, and K. Lean, 2016: AMVs in the Tropics:  
599 use in NWP, data quality and impact, Joint ECMWF/ESA Workshop on 'Tropical modeling,  
600 observations and data assimilation [Available online at <https://www.ecmwf.int/node/16865>]
- 601 Dee, D. P., S. M. Uppala, A. J. Simmons, P. Berrisford, P. Poli, S. Kobayashi, U. Andrae, M. A.  
602 Balmaseda, G. Balsamo, P. Bauer, P. Bechtold, A. C. M. Beljaars, L. van de Berg, J. Bidlot, N.  
603 Bormann, C. Delsol, R. Dragani, M. Fuentes, A. J. Geer, L. Haimberger, S. B. Healy, H.



- 604 Hersbach, E. V. Hólm, L. Isaksen, P. Kållberg, M. Köhler, M. Matricardi, A. P. McNally, B. M.  
605 Monge-Sanz, J.-J. Morcrette, B.-K. Park, C. Peubey, P. de Rosnay, C. Tavolato, J.-N. Thépaut,  
606 and F. Vitart, 2011: The ERA-Interim reanalysis: configuration and performance of the data  
607 assimilation system. *Q. J. R. Meteorol. Soc.*, **137**, 553–597. doi: 10.1002/qj.828
- 608 Dee, D. P., S. M. Uppala, A. J. Simmons, P. Berrisford, P. Poli, S. Kobayashi, U. Andrae, M. A.  
609 Balmaseda, G. Balsamo, P. Bauer, P. Bechtold, A. C. M. Beljaars, L. van de Berg, J. Bidlot, N.  
610 Bormann, C. Delsol, R. Dragani, M. Fuentes, A. J. Geer, L. Haimberger, S. B. Healy, H.  
611 Hersbach, E. V. Hólm, L. Isaksen, P. Kållberg, M. Köhler, M. Matricardi, A. P. McNally, B. M.  
612 Monge-Sanz, J.-J. Morcrette, B.-K. Park, C. Peubey, P. de Rosnay, C. Tavolato, J.-N. Thépaut,  
613 and F. Vitart, 2011: The ERA-Interim reanalysis: configuration and performance of the data  
614 assimilation system. *Q. J. R. Meteorol. Soc.*, **137**, 553–597. doi: 10.1002/qj.828
- 615 Ebert, E. E., 2008: Fuzzy verification of high-resolution gridded forecasts: a review and proposed  
616 framework. *Meteorological Applications: A journal of forecasting, practical applications,*  
617 *training techniques and modelling*, **15**(1), 51-64.
- 618 Fukui, S., T. Iwasaki, K. Saito, H. Seko, and M. Kunii, 2018: A feasibility study on the high-resolution  
619 regional reanalysis over Japan assimilating only conventional observations as an alternative to  
620 the dynamical downscaling. *Journal of the Meteorological Society of Japan*. **96**(6), 565-585.
- 621 Gibson, J. K., P. Kållberg, S. Uppala, A. Nomura, A. Hernandez, E. Serrano, 1997: ERA  
622 Description. *ECMWF Re-Analysis Final Report Series*, **1**, 71pp.
- 623 Grell, G. A., and S. R. Freitas, 2014: A scale and aerosol aware stochastic convective parameterization  
624 for weather and air quality modeling. *Atmos. Chem. Phys*, **14**(10), 5233-5250.
- 625 Hersbach, H., B. Bell, P. Berrisford, S. Hirahara, A. Horányi, J. Muñoz-Sabater, J. Nicolas, C. Peubey,  
626 R. Radu, D. Schepers, A. Simmons, C. Soci, S. Abdalla, X. Abellan, G. Balsamo, P. Bechtold,  
627 G. Biavati, J. Bidlot, M. Bonavita, G. D. Chiara, P. Dahlgren, D. Dee, M. Diamantakis, R.  
628 Dragani, J. Flemming, R. Forbes, M. Fuentes, A. Geer, L. Haimberger, S. Healy, R. J. Hogan, E.  
629 Hólm, M. Janisková, S. Keeley, P. Laloyaux, P. Lopez, C. Lupu, G. Radnoti, P. de Rosnay, I.  
630 Rozum, F. Vamborg, S. Villaume, and J.-N. Thépaut, 2020: The ERA5 global reanalysis.



- 631 *Quarterly Journal of the Royal Meteorological Society*, **146**(730), 1999-2049.
- 632 Hersbach, H., P. de Rosnay, B. Bell, D. Schepers, A. Simmons, C. Soci, S. Abdalla, M. Alonso  
633 Balmaseda, G. Balsamo, P. Bechtold, P. Berrisford, J. Bidlot, Eric. de Boissésou, M. Bonavita,  
634 P. Browne, R. Buizza, P. Dahlgren, D. Dee, R. Dragani, M. Diamantakis, J. Flemming, R. Forbes,  
635 A. Geer, T. Haiden, E. Hólm, L. Haimberger, R. Hogan, A. Horányi, M. Janisková, P. Laloyaux,  
636 P. Lopez, J. Muñoz-Sabater, C. Peubey, R. Radu, D. Richardson, J.-N. Thépaut, F. Vitart, X.  
637 Yang, E. Zsótér, and H. Zuo, 2018: Operational global reanalysis: progress, future directions  
638 and synergies with NWP, *ECMWF ERA report series*, N27.
- 639 Hong, S.-Y., Y. Noh, and J. Dudhia, 2006: A new vertical diffusion package with an explicit treatment  
640 of entrainment processes. *Monthly Weather Review*, **134**(9), 2318-2341.
- 641 Houtekamer, P. L., and F. Zhang, 2016: Review of the ensemble Kalman filter for atmospheric data  
642 assimilation. *Monthly Weather Review*, **144**(12), 4489-4532.
- 643 Iacono, M. J., J. S. Delamere, E. J. Mlawer, M. W. Shephard, S. A. Clough, and W. D. Collins, 2008:  
644 Radiative forcing by long-lived greenhouse gases: Calculations with the AER radiative transfer  
645 models. *Journal of Geophysical Research: Atmospheres*, **113**(D13).
- 646 Jermeý, P. M., and R. J. Renshaw, 2016: Precipitation representation over a two-year period in regional  
647 reanalysis. *Q. J. R. Meteorol. Soc.*, **142**, 1300-1310.
- 648 Jiménez, P. A., J. Dudhia, J. F. González-Rouco, J. Navarro, J. P. Montávez, and E. García-Bustamante,  
649 2012: A revised scheme for the WRF surface layer formulation. *Mon. Wea. Rev.*, **140**(3), 898-  
650 918.
- 651 Kalnay, E., M. Kanamitsu, R. Kistler, W. Collins, D. Deaven, L. Gandin, M. Iredell, S. Saha, G. White,  
652 J. Woollen, Y. Zhu, M. Chelliah, W. Ebisuzaki, W. Higgins, J. Janowiak, K. C. Mo, C. Ropelewski,  
653 J. Wang, A. Leetmaa, R. Reynolds, Roy Jenne and Dennis Joseph, 1996: The NCEP/NCAR 40-  
654 year reanalysis project. *Bull. Amer. Meteorol. Soc.*, **77**, 437-471.
- 655 Kanamitsu, M., W. Ebisuzaki, J. Woollen, S.-K. Yang, J. J. Hnilo, M. Fiorino, and G. L. Potter, 2002:  
656 NCEP–DOE AMIP-II Reanalysis (R-2). *Bull. Amer. Meteor. Soc.*, **83**, 1631–1643.
- 657 Kay, J. K., H. M. Kim, Y.-Y. Park, and J. Son, 2013: Effect of doubling ensemble size on the



- 658 performance of ensemble prediction in warm season using MOGREPS implemented in  
659 KMA, *Advances in Atmospheric Sciences*, **30**(5), 1287-1302, doi:10.1007/s00376-012-2083-y.
- 660 Kim, S., H. M. Kim, J. K. Kay, and S.-W. Lee, 2015: Development and evaluation of high resolution  
661 limited area ensemble prediction system in KMA, *Atmosphere*, **25**(1), 67-83. (in Korean with  
662 English abstract)
- 663 Kim, S., and H. M. Kim, 2017: Effect of considering sub-grid scale uncertainties on the forecasts of a  
664 high-resolution limited area ensemble prediction system, *Pure and Applied Geophysics*, **174**(5),  
665 2021-2037, doi: 10.1007/s00024-017-1513-2.
- 666 Kistler, R., W. Collins, S. Saha, G. White, J. Woollen, E. Kalnay, M. Chelliah, W. Ebisuzaki, M.  
667 Kanamitsu, V. Kousky, H. v. d. Dool, R. Jenne, and M. Fiorino, 2001: The NCEP–NCAR 50–  
668 Year Reanalysis: Monthly Means CD–ROM and Documentation. *Bull. Amer. Meteor. Soc.*, **82**,  
669 247–267.
- 670 Kobayashi, S., Y. Ota, Y. Harada, A. Ebata, M. Moriya, H. Onoda, K. Onogi, H. Kamahori, C. Kobayashi,  
671 H. Endo, K. Miyaoka, and K. Takahashi, 2015: The JRA-55 reanalysis: General specifications  
672 and basic characteristics, *J. Meteorol. Soc. Jpn.*, **93**, 5-48.
- 673 Mesinger, F., G. DiMego, E. Kalnay, K. Mitchell, P. C. Shafran, W. Ebisuzaki, D. Jović, J. Woollen, E.  
674 Rogers, E. H. Berbery, M. B. Ek, Y. Fan, R. Grumbine, W. Higgins, H. Li, Y. Lin, G. Manikin,  
675 D. Parrish, and W. Shi, 2006: North American Regional Reanalysis. *Bull. Amer. Meteor. Soc.*,  
676 **87**, 343–360.
- 677 Mittermaier, M. P., 2014: A strategy for verifying near-convection-resolving model forecasts at  
678 observing sites. *Weather and Forecasting*, **29**(2), 185-204.
- 679 National Centers for Environmental Prediction/National Weather Service/NOAA/U.S. Department of  
680 Commerce, 2008: NCEP ADP Global Upper Air and Surface Weather Observations  
681 (PREPBUFR format). *Research Data Archive at the National Center for Atmospheric Research*,  
682 *Computational and Information Systems Laboratory*, Boulder, CO. [Available online at  
683 <https://doi.org/10.5065/Z83F-N512>.] Accessed 5 July 2018.
- 684 National Climatic Data Center/NESDIS/NOAA/U.S. Department of Commerce, Meteorology



- 685 Department/Florida State University, Climate Analysis Section/Climate and Global Dynamics  
686 Division/National Center for Atmospheric Research/University Corporation for Atmospheric  
687 Research, and Harvard College Observatory/Harvard University, 1981: World Monthly Surface  
688 Station Climatology. *Research Data Archive at the National Center for Atmospheric Research,*  
689 *Computational and Information Systems Laboratory*, Boulder, CO. [Available online at  
690 <http://rda.ucar.edu/datasets/ds570.0/>.] Accessed 7 Nov 2019.
- 691 On, N., H. M. Kim, and S. Kim, 2018: Effects of resolution, cumulus parameterization scheme,  
692 and probability forecasting on precipitation forecasts in a high-resolution limited-area  
693 ensemble prediction system, *Asia-Pacific Journal of Atmospheric Sciences*, **54**, 623-  
694 637, doi:10.1007/s13143-018-0081-4.
- 695 Onogi, K., J. Tsutsui, H. Koide, M. Sakamoto, S. Kobayashi, H. Hatsushika, T. Matsumoto, N.  
696 Yamazaki, H. Kamahori, K. Takahashi, S. Kadokura, K. Wada, K. Kato, R. Oyama, T.  
697 Ose, N. Mannoji, and R. Taira, 2007: The JRA-25 reanalysis. *J. Meteor. Soc. Japan*, **85**,  
698 369–432.
- 699 Park, J., and H. M. Kim, 2020: Design and evaluation of CO<sub>2</sub> observation network to optimize surface  
700 CO<sub>2</sub> fluxes in Asia using observation system simulation experiments, *Atmospheric Chemistry*  
701 *and Physics*, **20**, 5175-5195, <https://doi.org/10.5194/acp-20-5175-2020>.
- 702 Penny, S. G., 2014: The hybrid local ensemble transform Kalman filter. *Monthly Weather Review*,  
703 **142**(6), 2139-2149.
- 704 Penny, S. G., D. W. Behringer, J. A. Carton, and E. Kalnay, 2015: A hybrid global ocean data  
705 assimilation system at NCEP. *Monthly Weather Review*, **143**(11), 4660-4677.
- 706 Que, L. J., W. L. Que, and J. M. Feng, 2016: Intercomparison of different physics schemes in the WRF  
707 model over the Asian summer monsoon region. *Atmospheric and Oceanic Science Letters*, **9**(3),  
708 169-177.
- 709 Renshaw, R., P. Jerney, D. Barker, A. Maycock, and S. Oxley, 2013: EURO4M regional reanalysis  
710 system, *Forecasting Research Technical Report*, No. **583**, Met Office.



- 711 Rienecker, M. M., M. J. Suarez, R. Gelaro, R. Todling, J. Bacmeister, E. Liu, M. G. Bosilovich, S. D.  
712 Schubert, L. Takacs, G.-K. Kim, S. Bloom, J. Chen, D. Collins, A. Conaty, A. da Silva, W. Gu,  
713 J. Joiner, R. D. Koster, R. Lucchesi, A. Molod, T. Owens, S. Pawson, P. Pegion, C. R. Redder,  
714 R. Reichle, F. R. Robertson, A. G. Ruddick, M. Sienkiewicz, and J. Woollen, 2011: MERRA:  
715 NASA's Modern-Era Retrospective Analysis for Research and Applications. *J. Climate*, **24**,  
716 3624–3648.
- 717 Saha, S., S. Moorthi, H.-L. Pan, X. Wu, J. Wang, S. Nadiga, P. Tripp, R. Kistler, J. Woollen, D. Behringer,  
718 H. Liu, D. Stokes, R. Grumbine, G. Gayno, J. Wang, Y.-T. Hou, H.-Y. Chuang, H.-M. H. Juang,  
719 J. Sela, M. Iredell, R. Treadon, D. Kleist, P. V. Delst, D. Keyser, J. Derber, M. Ek, J. Meng, H.  
720 Wei, R. Yang, S. Lord, H. V. D. Dool, A. Kumar, W. Wang, C. Long, M. Chelliah, Y. Xue, B.  
721 Huang, J.-K. Schemm, W. Ebisuzaki, R. Lin, P. Xie, M. Chen, S. Zhou, W. Higgins, C.-Z. Zou,  
722 Q. Liu, Y. Chen, Y. Han, L. Cucurull, R. W. Reynolds, G. Rutledge, and M. Goldberg, 2010: The  
723 NCEP Climate Forecast System Reanalysis. *Bull. Amer. Meteor. Soc.*, **91**, 1015–1057.
- 724 Schubert, S., J. Pfaendtner, and R. Rood, 1993: An assimilated dataset for earth science applications.  
725 *Bull. Amer. Meteor. Soc.*, **74**, 2331–2342.
- 726 Shiferaw, A., T. Tadesse, C. Rowe, and R. Oglesby, 2018: Precipitation extremes in dynamically  
727 downscaled climate scenarios over the greater horn of Africa. *Atmosphere*, **9**(3), 112.
- 728 Shin, I.-C, J.-G. Kim, C.-Y. Chung, S.-K. Baek, and J.-R. Lee, 2016: The impact of the COMS data on  
729 the KMA NWP System, *14th JCSDA Technical Review Meeting & Science Workshop on*  
730 *Satellite Data Assimilation*.
- 731 Skamarock, W. C., J. B. Klemp, J. Dudhia, D. O. Gill, D. M. Barker, M. G. Duda, X.-Y. Huang, W.  
732 Wang, J. G. Powers, 2008: A description of the advanced research WRF version 3. NCAR Tech.  
733 Note NCAR/TN-475+ STR Available at:  
734 <https://opensky.ucar.edu/islandora/object/technotes%3A500/datastream/PDF/view>.
- 735 Tewari, M., F. Chen, W. Wang, J. Dudhia, M. A. LeMone, K. Mitchell, M. Ek, G. Gayno, J. Wegiel, and  
736 R. H. Cuenca, 2004: Implementation and verification of the unified NOAA land surface model  
737 in the WRF model. *20th conference on weather analysis and forecasting/16th conference on*



- 738           *numerical weather prediction* (Vol. 1115). Seattle, WA: American Meteorological Society.
- 739   Theis, S. E., A. Hense, and U. Damrath, 2005: Probabilistic precipitation forecasts from a deterministic  
740           model: A pragmatic approach. *Meteorological Applications: A journal of forecasting, practical*  
741           *applications, training techniques and modelling*, **12**(3), 257-268.
- 742   Thompson, G., P. R. Field, R. M. Rasmussen, and W. D. Hall, 2008: Explicit forecasts of winter  
743           precipitation using an improved bulk microphysics scheme. Part II: Implementation of a new  
744           snow parameterization. *Mon. Wea. Rev.*, **136**(12), 5095-5115.
- 745   Uppala, S. M., P. W. Kållberg, A. J. Simmons, U. Andrae, V. D. C. Bechtold, M. Fiorino, J. K. Gibson,  
746           J. Haseler, A. Hernandez, G. A. Kelly, X. Li, K. Onogi, S. Saarinen, N. Sokka, R. P. Allan, E.  
747           Andersson, K. Arpe, M. A. Balmaseda, A. C. M. Beljaars, L. V. D. Berg, J. Bidlot, N. Bormann,  
748           S. Caires, F. Chevallier, A. Dethof, M. Dragosavac, M. Fisher, M. Fuentes, S. Hagemann, E.  
749           Hólm, B. J. Hoskins, L. Isaksen, P. A. E. M. Janssen, R. Jenne, A. P. McNally, J.-F. Mahfouf, J.-  
750           J. Morcrette, N. A. Rayner, R. W. Saunders, P. Simon, A. Sterl, K. E. Trenberth, A. Untch, D.  
751           Vasiljevic, P. Viterbo, and J. Woollen, 2005: The ERA-40 re-analysis. *Q. J. R. Meteorol. Soc.*,  
752           **131**: 2961–3012.
- 753   Warrick, F., 2015: Options for filling the LEO-GEO AMV Coverage Gap. *NWP SAF Tech. Doc.*, NWP  
754           SAF-MO-TR-030, 21 p.
- 755   Wilks, D. S., 2006: Statistical methods in the atmospheric sciences, 2nd edn., *Academic Press*, 627pp.
- 756   Wilson, L., 2010: Verification of severe weather forecasts in support of the “SWFDP Southern Africa”  
757           project. *Report for the World Meteorological Organisation*, pp. 21  
758           ([www.wmo.int/pages/prog/www/BAS/documents/Doc-7-Verification.doc](http://www.wmo.int/pages/prog/www/BAS/documents/Doc-7-Verification.doc))
- 759   Yang, E.-G., and H. M. Kim, 2017: Evaluation of a regional reanalysis and ERA-Interim over East Asia  
760           using in situ observations during 2013-14, *Journal of Applied Meteorology and*  
761           *Climatology*, **56**(10), 2821-2844,
- 762   Yang, E.-G., and H. M. Kim, 2019: Evaluation of Short-Range Precipitation Reforecasts from East Asia  
763           Regional Reanalysis. *Journal of Hydrometeorology*, **20**(2), 319-337.
- 764   Yang, E.-G., and H. M. Kim, 2021a: A comparison of variational, ensemble-based, and hybrid data



- 765            assimilation methods over East Asia for two one-month periods, *Atmospheric Research*, **249**,  
766            105257.
- 767    Yang, E.-G., and H. M. Kim, 2021b: East Asia Regional Reanalysis 6 hourly data on pressure levels  
768            from 2010 to 2019, <https://doi.org/10.7910/DVN/7P8MZT>, Harvard Dataverse, V1.
- 769    Yang, E.-G., and H. M. Kim, 2021c: East Asia Regional Reanalysis 6 hourly precipitation data from  
770            2010 to 2019, <https://doi.org/10.7910/DVN/Q07VRC>, Harvard Dataverse, V1.
- 771    Yoo, C., E. Cho, 2018: Comparison of GCM precipitation predictions with their RMSEs and pattern  
772            correlation coefficients. *Water*, **10**(1), 28.
- 773    Zhang, F., M. Zhang, and J. Poterjoy, 2013: E3DVar: Coupling an ensemble Kalman filter with three-  
774            dimensional variational data assimilation in a limited-area weather prediction model and  
775            comparison to E4DVar. *Monthly Weather Review*, **141**(3), 900-917.
- 776    Zhang, Q., Y. Pan, S. Wang, J. Xu, and J. Tang, 2017: High-resolution regional reanalysis in China:  
777            Evaluation of 1 year period experiments. *Journal of Geophysical Research: Atmospheres*,  
778            **122**(20), 10-801.
- 779



780 **Table caption**

781 Table 1. Model configuration

782 Table 2. The  $2 \times 2$  contingency table for dichotomous (yes-no) events.

783



784 **Figure caption**

785 Figure 1. The model domain over East Asia with verification area (black dashed box).

786 Figure 2. RMSEs of analysis of (a,b) zonal wind, (c,d) meridional wind, (e,f) temperature, and  
787 (g,h) Qvapor (water vapor mixing ratio) from ERA-I (black dashed), ERA5 (black solid),  
788 E3DVAR (blue dashed), AdvHG (blue solid) depending on pressure levels for (left) January  
789 and (right) July in 2017.

790 Figure 3. Same as Fig. 2 except for 24 h forecast.

791 Figure 4. Same as Fig. 2 except for 36 h forecast.

792 Figure 5. RMSEs of analysis of (a) zonal wind, (b) meridional wind, (c) temperature, and (d)  
793 Qvapor (water vapor mixing ratio) from ERA5 (black solid) and AdvHG (blue solid) and  
794 spreads of analysis (black dashed) and 6 h forecast (gray dashed) of AdvHG depending on  
795 pressure levels averaged over the two-year period of 2017–2018.

796 Figure 6. Same as Fig. 5 except for RMSE of 24 h forecast.

797 Figure 7. (a,c) ETS and (b,d) FBI for (a,b) January and (c,d) July in 2017 depending on  
798 thresholds 0.5, 1, 4, 8, and 16 mm (6 h)<sup>-1</sup>.

799 Figure 8. (a,c) POD and (b,d) FAR for (a,b) January and (c,d) July in 2017 depending on  
800 thresholds 0.5, 1, 4, 8, and 16 mm (6 h)<sup>-1</sup>.

801 Figure 9. Brier skill score of the probabilistic postprocessed forecast with reference to the  
802 WRF-based ERA-I for (a-d) January and (e-h) July in 2017 (Blue solid: AdvHG, blue dashed:  
803 E3DVAR, red solid: WRF-based ERA5).

804 Figure 10. The spatial distribution of 6 h accumulated precipitation of (1<sup>st</sup> column) observation,  
805 (2<sup>nd</sup> column) E3DVAR, (3<sup>rd</sup> column) AdvHG, (4<sup>th</sup> column) ERA-I, (5<sup>th</sup> column) ERA5, (6<sup>th</sup>



806 column) ERA-I\_fromECMWF, and (7<sup>th</sup> column) ERA5\_fromECMWF and the pattern  
807 correlation coefficient (PCC) shown at the bottom right of each figure at valid time (1<sup>st</sup> low, 3<sup>rd</sup>  
808 low) 06 UTC and (2<sup>nd</sup> low, 4<sup>th</sup> low) 18 UTC on 29<sup>th</sup> and 30<sup>th</sup> of January in 2017.

809 Figure 11. As in Fig. 10, but for 1<sup>st</sup> and 2<sup>nd</sup> of July in 2017.

810 Figure 12. The spatial distribution of the monthly accumulated precipitation of (a) observations,  
811 (b) E3DVAR, (c) AdvHG, (d) ERA-I, (e) ERA5, (f) ERA-I from ECMWF, and (g) ERA5 from  
812 ECMWF for January 2017.

813 Figure 13. As in Fig. 12, but for July 2017.

814



815 Table 1. Model configuration

	Description
<b>Hori. Resol.</b>	12 km (540×432 grid points)
<b>Vert. Lev.</b>	50 vertical levels (up to 5 hPa)
<b>Model</b>	WRF Model (v3.7.1, Skamarock et al. 2008)
<b>LBC</b>	ERA5 (Hersbach et al. 2020)
<b>Data assimilation</b>	E3DVAR (Zhang et al. 2013), Advanced hybrid gain method
<b>Microphysics</b>	Thompson scheme (Thompson et al. 2008)
<b>Cumulus convection</b>	Grell–Freitas ensemble scheme (Grell and Freitas 2014)
<b>PBL</b>	Yonsei University scheme (Hong et al. 2006)
<b>Radiation</b>	Rapid Radiative Transfer Model (RRTMG) scheme (Iacono et al. 2008)
<b>Surface layer</b>	Revised MM5 Monin–Obukhov scheme (Jiménez et al. 2012)
<b>Surface model</b>	Unified Noah Land Surface Model (Tewari et al. 2004)

816

817

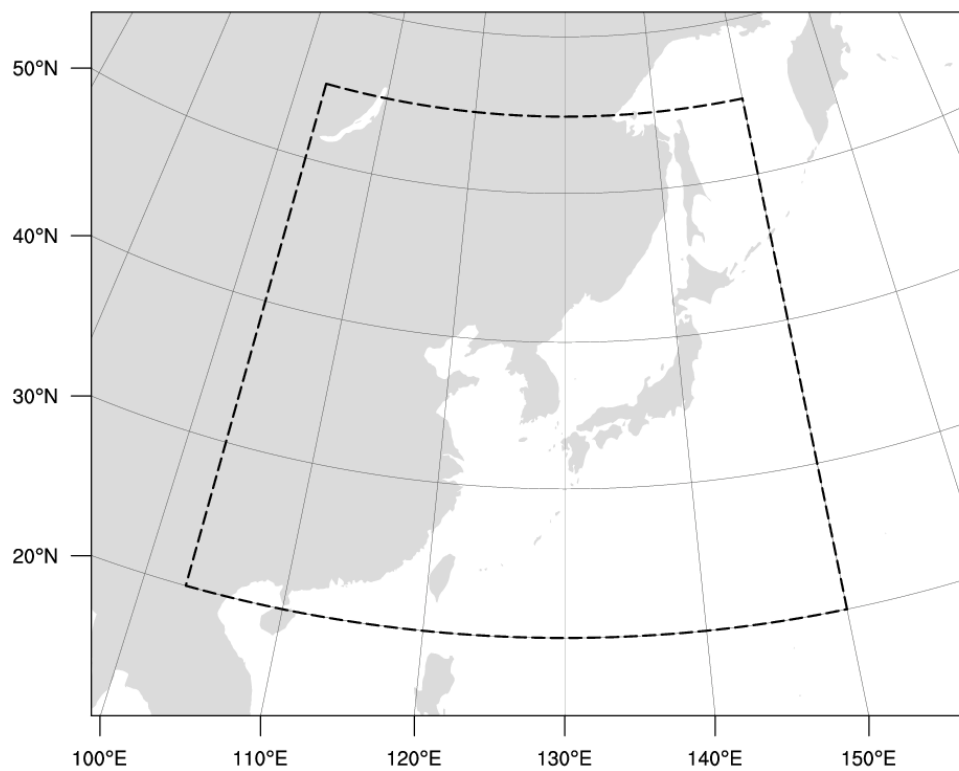


818 Table 2. The  $2 \times 2$  contingency table for dichotomous (yes-no) events.

Forecast	Observed		
	Yes	No	
Yes	Hits (A)	False alarms (B)	A + B
No	Misses (C)	Correct rejections (D)	C + D
	A + C	B + D	Total = A + B + C + D

819

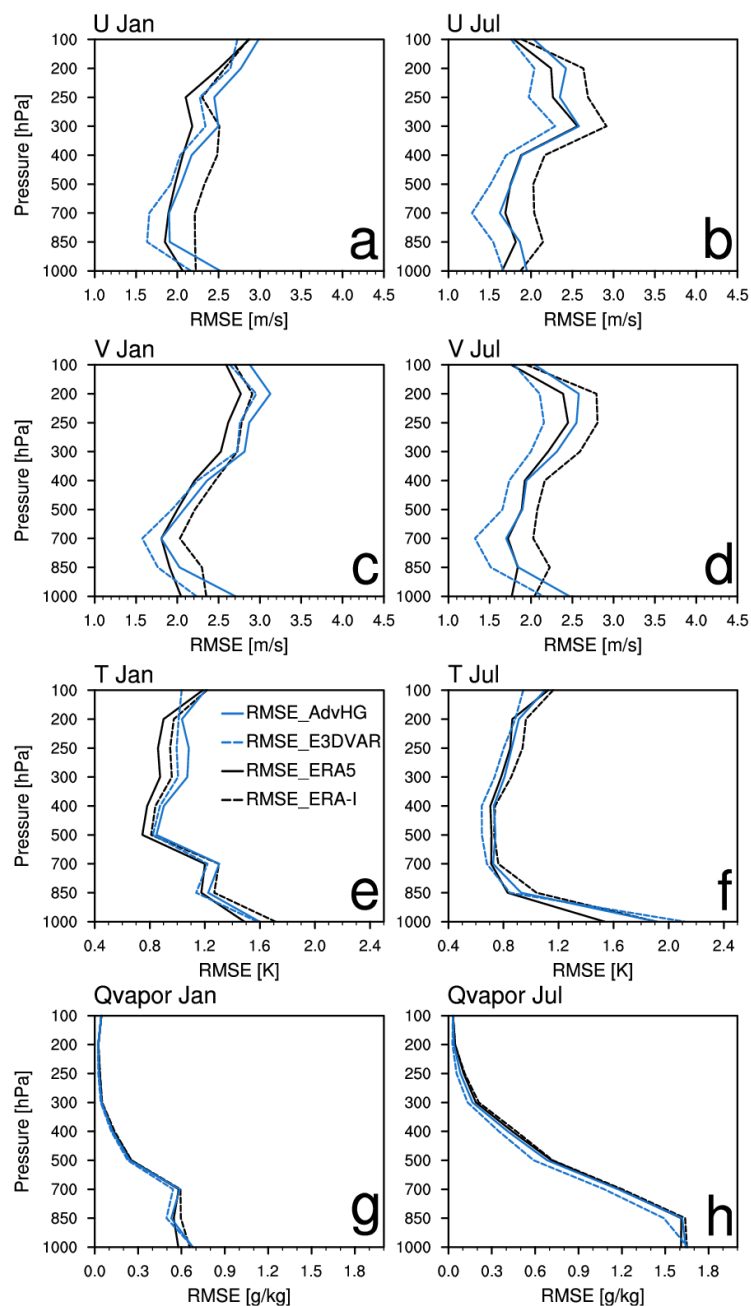
820



821

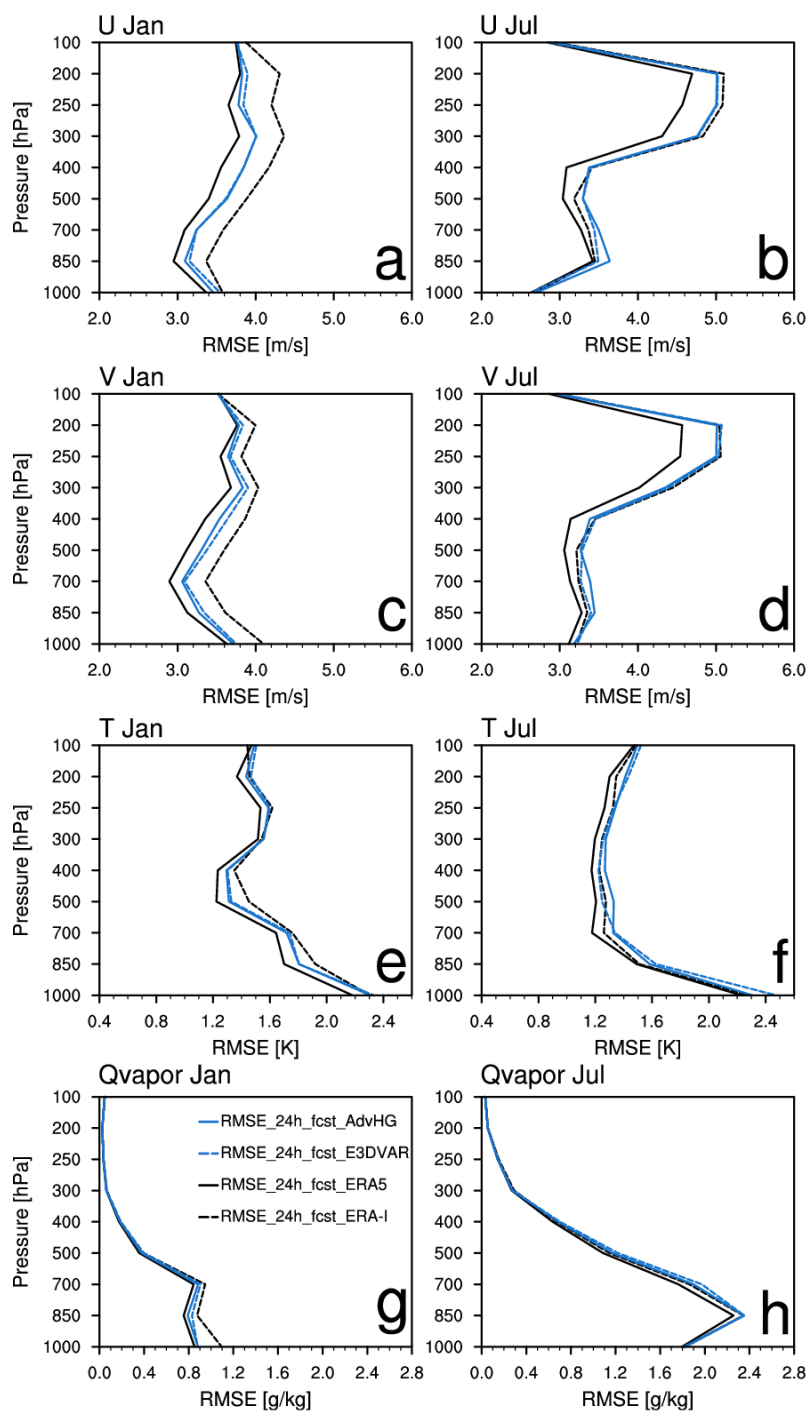
822 Figure 1. The model domain over East Asia with verification area (black dashed box).

823



824

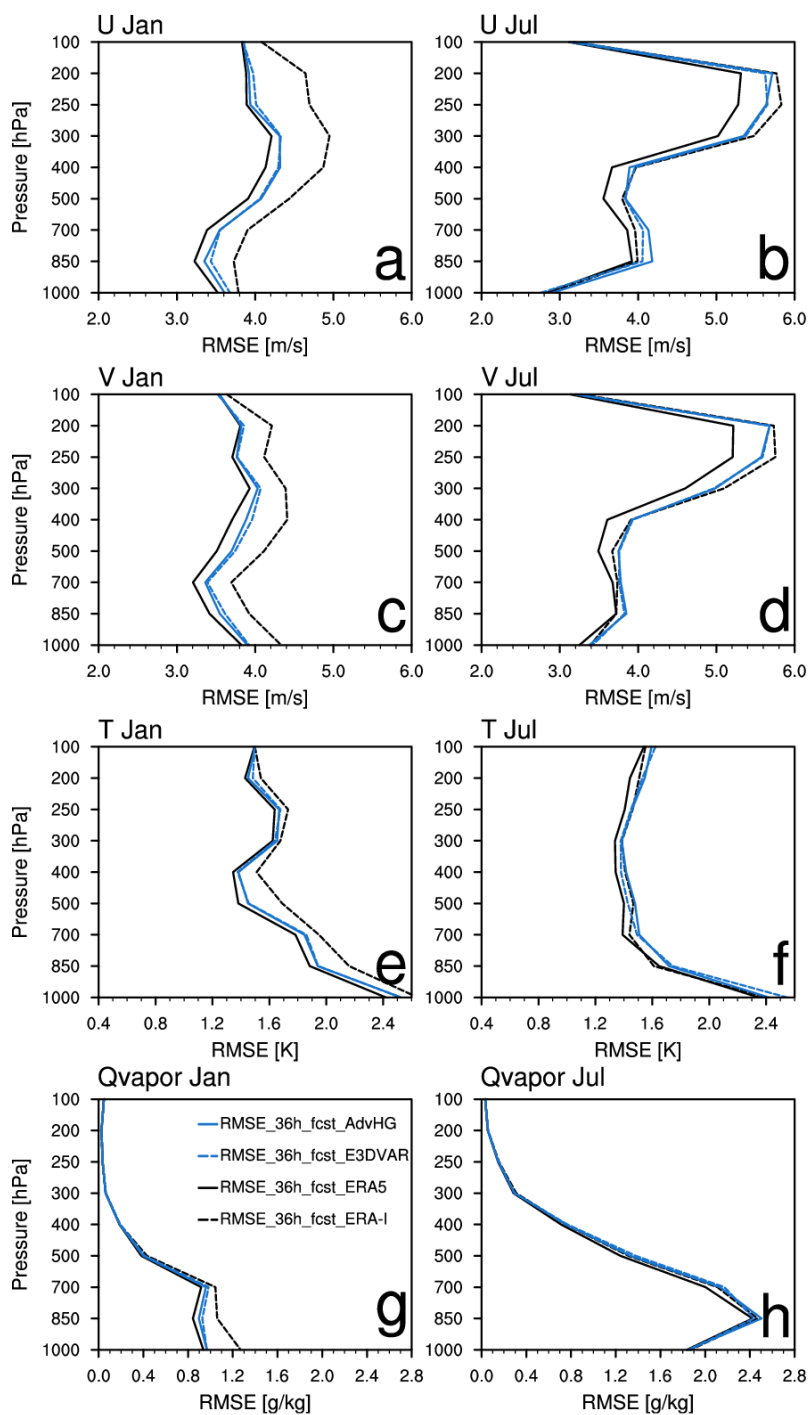
825 Figure 2. RMSEs of analysis of (a,b) zonal wind, (c,d) meridional wind, (e,f) temperature, and  
826 (g,h) Qvapor (water vapor mixing ratio) from ERA-I (black dashed), ERA5 (black solid),  
827 E3DVAR (blue dashed), AdvHG (blue solid) depending on pressure levels for (left) January  
828 and (right) July in 2017.



829

830

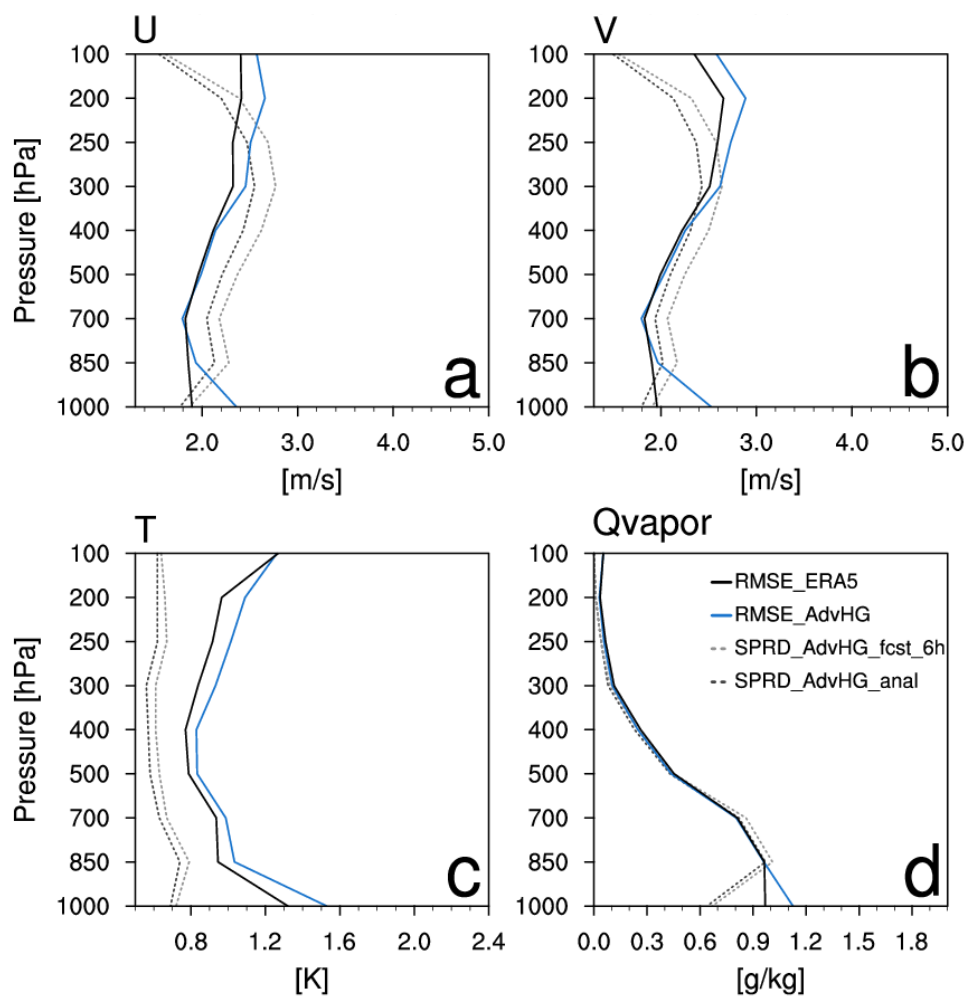
Figure 3. Same as Fig. 2 except for 24 h forecast.



831

832

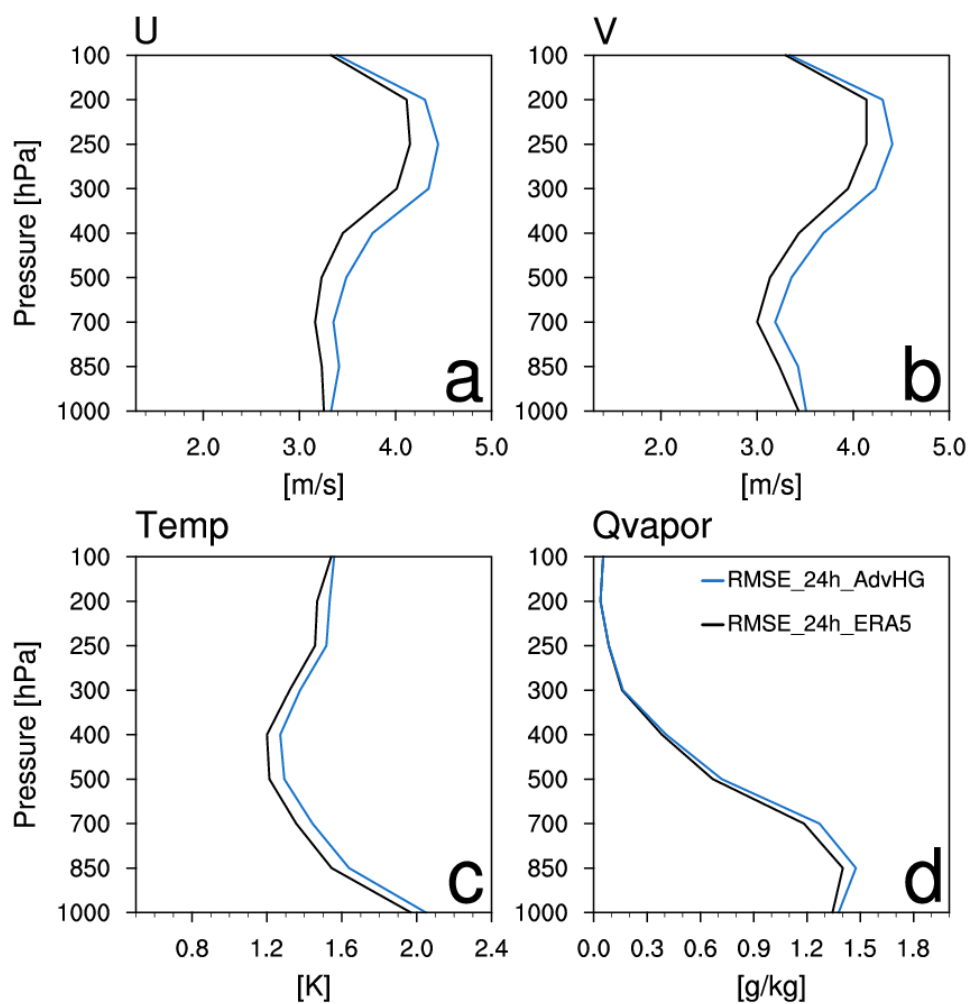
Figure 4. Same as Fig. 2 except for 36 h forecast.



833

834 Figure 5. RMSEs of analysis of (a) zonal wind, (b) meridional wind, (c) temperature, and (d)  
835 Qvapor (water vapor mixing ratio) from ERA5 (black solid) and AdvHG (blue solid) and  
836 spreads of analysis (black dashed) and 6 h forecast (gray dashed) of AdvHG depending on  
837 pressure levels averaged over the two-year period of 2017–2018.

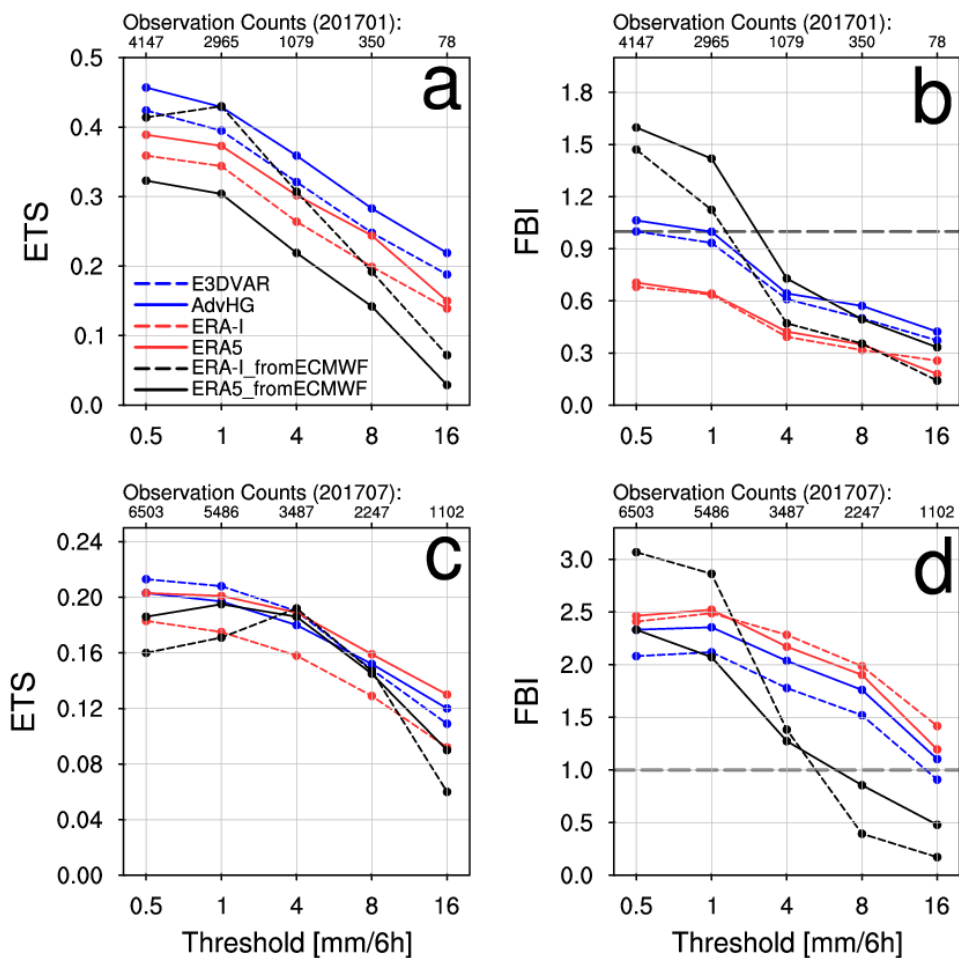
838



839

840 Figure 6. Same as Fig. 5 except for RMSE of 24 h forecast.

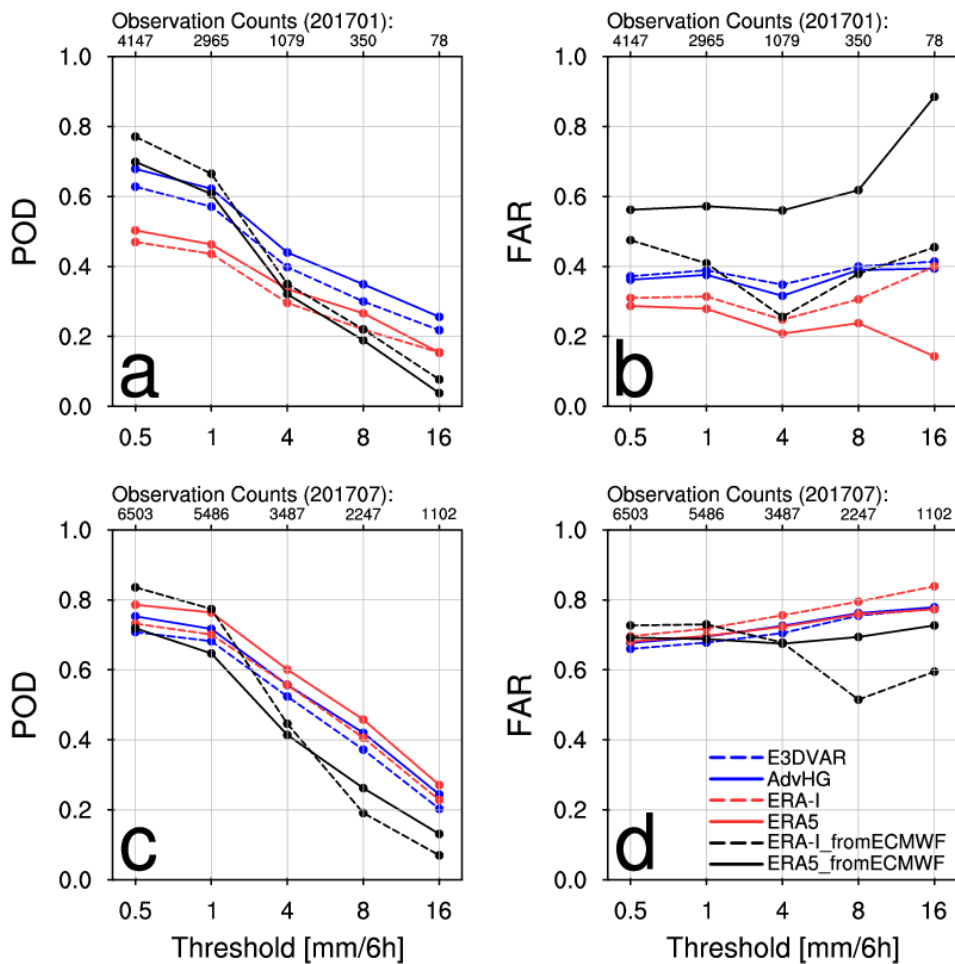
841



842

843 Figure 7. (a,c) ETS and (b,d) FBI for (a,b) January and (c,d) July in 2017 depending on  
 844 thresholds 0.5, 1, 4, 8, and 16 mm (6 h)<sup>-1</sup>.

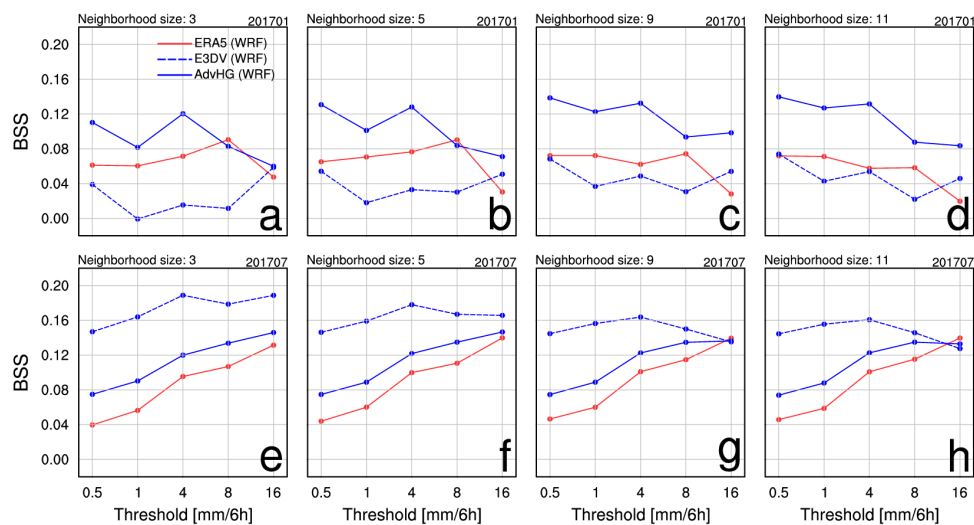
845



846

847 Figure 8. (a,c) POD and (b,d) FAR for (a,b) January and (c,d) July in 2017 depending on  
 848 thresholds 0.5, 1, 4, 8, and 16 mm (6 h)<sup>-1</sup>.

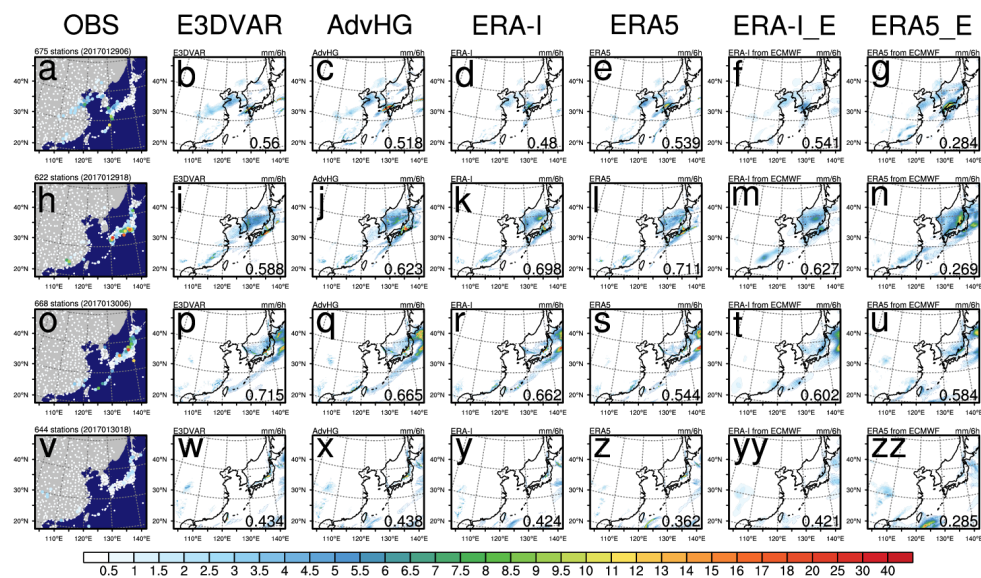
849



850

851 Figure 9. Brier skill score of the probabilistic postprocessed forecast with reference to the  
852 WRF-based ERA-I for (a-d) January and (e-h) July in 2017 (Blue solid: AdvHG, blue dashed:  
853 E3DVAR, red solid: WRF-based ERA5).

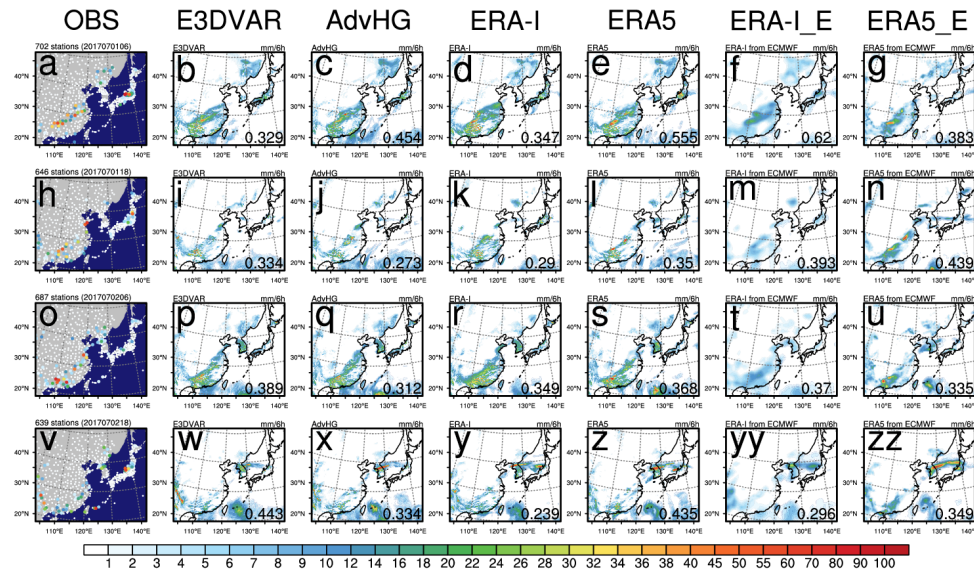
854



855

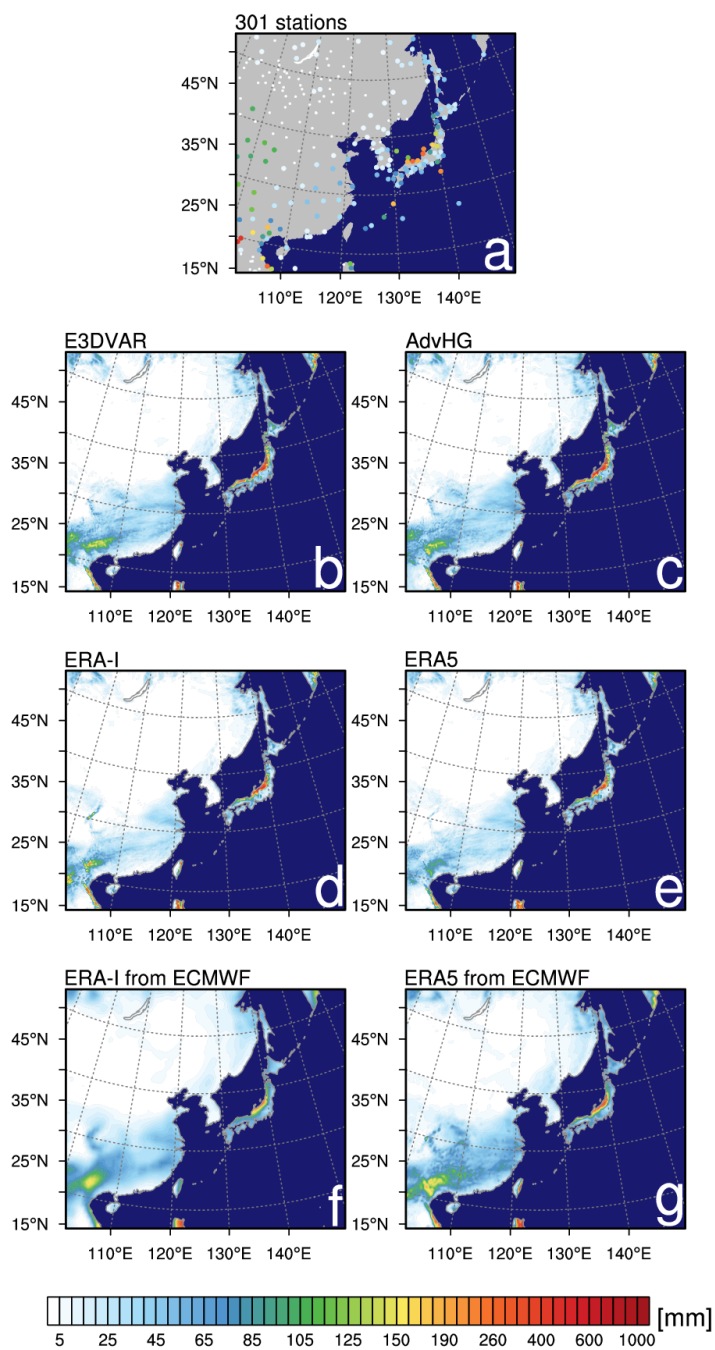
856 Figure 10. The spatial distribution of 6 h accumulated precipitation of (1<sup>st</sup> column) observation,  
857 (2<sup>nd</sup> column) E3DVAR, (3<sup>rd</sup> column) AdvHG, (4<sup>th</sup> column) ERA-I, (5<sup>th</sup> column) ERA5, (6<sup>th</sup>  
858 column) ERA-I\_fromECMWF, and (7<sup>th</sup> column) ERA5\_fromECMWF and the pattern  
859 correlation coefficient (PCC) shown at the bottom right of each figure at valid time (1<sup>st</sup> low, 3<sup>rd</sup>  
860 low) 06 UTC and (2<sup>nd</sup> low, 4<sup>th</sup> low) 18 UTC on 29<sup>th</sup> and 30<sup>th</sup> of January in 2017.

861



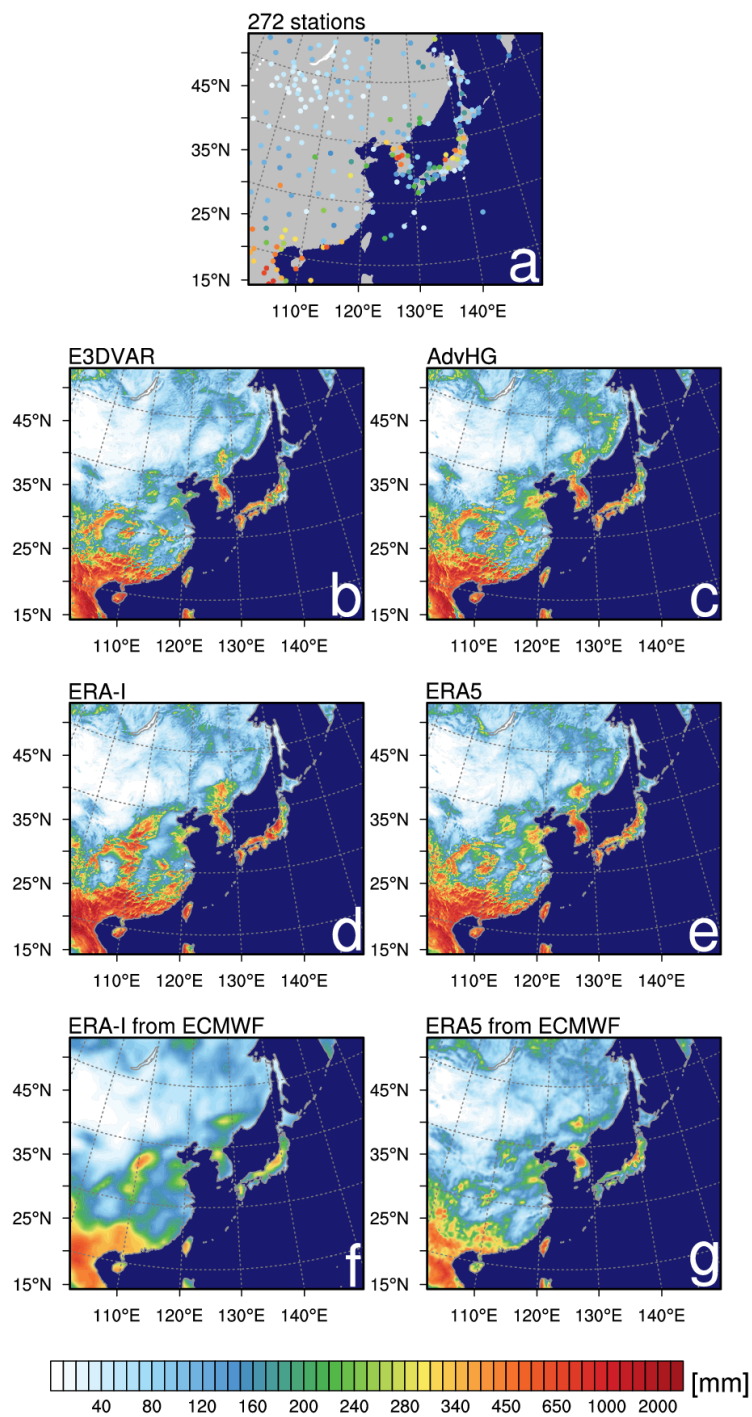
862

863 Figure 11. As in Fig. 10, but for 1<sup>st</sup> and 2<sup>nd</sup> of July in 2017.



864

865 Figure 12. The spatial distribution of the monthly accumulated precipitation of (a) observations,  
866 (b) E3DVAR, (c) AdvHG, (d) ERA-I, (e) ERA5, (f) ERA-I from ECMWF, and (g) ERA5 from  
867 ECMWF for January 2017.



868

869 Figure 13. As in Fig. 12, but for July 2017.